The K^+ channel $K_{IR}2.1$ functions in tandem with proton influx to mediate sour taste transduction

Wenlei Ye[a], Rui B. Chang[a,1], Jeremy D. Bushman[a], Yu-Hsiang Tu[a], Eric M. Mulhall[a], Courtney E. Wilson[b,c], Alexander J. Cooper[a], Wallace S. Chick[d], David C. Hill-Eubanks[e], Mark T. Nelson[e,f], Sue C. Kinnamon[b,c], and Emily R. Liman[a,2]

[a]Section of Neurobiology, Department of Biological Sciences, University of Southern California, Los Angeles, CA 90089; [b]Department of Otolaryngology, University of Colorado Medical School, Aurora, CO 80045; [c]Rocky Mountain Taste and Smell Center, University of Colorado Medical School, Aurora, CO 80045; [d]Department of Cell and Developmental Biology, University of Colorado Medical School, Aurora, CO 80045; [e]Department of Pharmacology, University of Vermont, Burlington, VT 05405; and [f]Institute of Cardiovascular Sciences, University of Manchester, Manchester M13 9PT, United Kingdom

Edited by King-Wai Yau, Johns Hopkins University School of Medicine, Baltimore, MD, and approved October 21, 2015 (received for review July 20, 2015)

Sour taste is detected by a subset of taste cells on the tongue and palate epithelium that respond to acids with trains of action potentials. Entry of protons through a Zn^{2+}-sensitive proton conductance that is specific to sour taste cells has been shown to be the initial event in sour taste transduction. Whether this conductance acts in concert with other channels sensitive to changes in intracellular pH, however, is not known. Here, we show that intracellular acidification generates excitatory responses in sour taste cells, which can be attributed to block of a resting K^+ current. We identify $K_{IR}2.1$ as the acid-sensitive K^+ channel in sour taste cells using pharmacological and RNA expression profiling and confirm its contribution to sour taste with tissue-specific knockout of the *Kcnj2* gene. Surprisingly, acid sensitivity is not conferred on sour taste cells by the specific expression of $K_{IR}2.1$, but by the relatively small magnitude of the current, which makes the cells exquisitely sensitive to changes in intracellular pH. Consistent with a role of the K^+ current in amplifying the sensory response, entry of protons through the Zn^{2+}-sensitive conductance produces a transient block of the $K_{IR}2.1$ current. The identification in sour taste cells of an acid-sensitive K^+ channel suggests a mechanism for amplification of sour taste and may explain why weak acids that produce intracellular acidification, such as acetic acid, taste more sour than strong acids.

proton channel | taste cell | gustatory | inward rectifier | potassium channel

Sour taste is mediated by a subset of taste cells on the tongue and palate epithelium that respond to acids with trains of action potentials and transmitter release (1–3). Both strong acids, such as hydrochloric acid, and weak acids, such as acetic or citric acid, produce a sour sensation in humans and evoke sensory responses in nerve recordings in a variety of model organisms, including rat, mouse, and hamster (4–7). A number of molecules have been proposed to transduce sour taste, most recently the ion channel PKD2L1/PKD1L3 (8–12), but their role in taste transduction remains unclear as subsequent studies using knockout mouse strains have failed to identify significant effects on sour taste (13–15). Nonetheless, the *Pkd2l1* gene serves as a useful marker for sour taste cells (also designated type III cells), which account for ∼10% of the ∼50–100 taste cells found in each taste bud (1, 9, 11, 16, 17). Previously, using a *Pkd2l1*-YFP mouse, we showed that sour cells express a unique Zn^{2+}-sensitive proton conductance, of unknown identity, that is likely to mediate the initial event in taste transduction (16). Whether this conductance acts "alone" or in concert with other channels sensitive to changes in intracellular pH is not known. In this report, we provide evidence for a second component of the transduction cascade: a resting K^+ current, mediated by $K_{IR}2.1$ channels, which have an unexpected sensitivity to intracellular pH.

Several pieces of evidence argue for a second component of taste transduction, sensitive to intracellular acidification. First, it was demonstrated nearly a century ago (18) that weak acids, which can penetrate the cell membrane and acidify the cell cytosol, taste more sour than strong acids, at the same pH. Mirroring this effect, it is well established that the gustatory nerve response is greater when the tongue is stimulated with weak acids than with strong acids at the same pH, and varies both as a factor of pH and of the concentration of the undissociated acid (5, 19). Similarly, calcium responses from sour-sensitive cells in slice recording can be evoked with weak acids at a higher pH compared with strong acids (20). Moreover, we previously reported that action potentials can be elicited in sour taste cells in response to extracellular pH of 6.5–6.7, where the current carried by protons (2–3 pA) is unlikely to be sufficient to depolarize the cell (21). All of these phenomena can be explained if intracellular acidification increases membrane excitability of sour taste cells. Indeed, it has been proposed that two-pore domain K^+ channels, several of which are expressed at high levels in sour taste cells, could serve as sensors of intracellular pH (22, 23). However, to date, there is no direct evidence showing that sour taste cells are activated by intracellular acidification, and the molecular mechanisms by which intracellular acidification could excite sour taste cells remain largely unexplored.

Here, using genetically identified sour taste cells, we show that intracellular acidification, in the absence of extracellular acidification, is sufficient to produce robust trains of action potentials in sour taste cells but not in taste cells that detect bitter, sweet, and umami. Intracellular acidification blocks an inwardly rectifying K^+ current in sour taste cells, which we identify as $K_{IR}2.1$

Significance

Among the five basic tastes, sour is one of the least understood. Notably, the sour receptor remains to be identified, and molecular mechanisms by which sour stimuli are detected are largely not known. Previous work has shown that H^+ ions can directly enter sour taste cells, eliciting a change in membrane potential and acidification of the cell cytosol. In the present work, we identify a second element of sensory transduction, a K^+ channel, $K_{IR}2.1$, which is inhibited by intracellular acidification. The presence of an acid-sensitive K^+ channel in sour taste cells allows for amplification of the sensory response and may explain why weak acids that produce intracellular acidification, such as acetic acid, taste more sour than strong acids.

Author contributions: W.Y., R.B.C., J.D.B., Y.-H.T., E.M.M., C.E.W., A.J.C., M.T.N., S.C.K., and E.R.L. designed research; W.Y., R.B.C., J.D.B., Y.-H.T., E.M.M., C.E.W., A.J.C., and E.R.L. performed research; W.S.C., D.C.H.-E., M.T.N., and S.C.K. contributed new reagents/analytic tools; W.Y., R.B.C., J.D.B., Y.-H.T., E.M.M., C.E.W., A.J.C., M.T.N., S.C.K., and E.R.L. analyzed data; and W.Y., R.B.C., J.D.B., M.T.N., S.C.K., and E.R.L. wrote the paper.

The authors declare no conflict of interest.

This article is a PNAS Direct Submission.

Freely available online through the PNAS open access option.

See Commentary on page 246.

[1]Present address: Department of Cell Biology, Harvard Medical School, Boston, MA 02115.

[2]To whom correspondence should be addressed. Email: liman@USC.edu.

This article contains supporting information online at www.pnas.org/lookup/suppl/doi:10.1073/pnas.1514282112/-/DCSupplemental.

based on expression profiling and pharmacological analysis, and confirm using a newly developed, cell-type–specific $K_{IR}2.1$-knockout model. We propose that block of the resting K^+ current in sour taste cells contributes to the taste of weak acids and provides a mechanism for amplification of the sensory response.

Results

Sour Taste Cells Respond to Intracellular Acidification with Action Potentials. To determine whether sour taste cells respond electrically to intracellular acidification, we measured action potentials in cell-attached recording from freshly isolated taste receptor cells from mouse circumvallate papillae (CV). Sour taste cells were identified by expression of YFP from the *Pkd2l1* promoter (PKD2L1 cells), and responses were compared with those obtained from nonsour taste cells, identified by GFP expression from the *Trpm5* (transient receptor potential M5) promoter in a double-transgenic mouse (24, 25). Healthy, electrically excitable cells were identified using 2 mM Ba^{2+}, which blocks resting K^+ channels and elicits action potentials in both cell types (Fig. 1 *A* and *B*). To acidify the cell cytosol, we used acetic acid (AA) and propionic acid (PA), weak acids that partition in the lipid bilayer in their protonated form and are able to shuttle protons across the cell membrane (26–28). Each acid was used at a concentration of 100 mM and pH of 7.4, which generates ∼0.3 mM of the membrane permeable form. As can be seen in Fig. 1 *A* and *B*, the two weak acids evoked robust action potential firing in PKD2L1 cells, whereas no action potentials were elicited in response to the two weak acids in TRPM5 cells. As a control for removal of Cl^-, we used methane sulfonic acid (MA), which is a strong acid and cannot shuttle protons across the cell membrane. MA was without effect on PKD2L1 cells (Fig. 1 *A* and *B*). We also measured responses from PKD2L1 cells isolated from foliate (FL) papillae on the sides of the tongue, and compared the results with those obtained using cells isolated from the CV (Fig. S1); no difference in responses were detected; thus, all additional experiments were done using cells from the CV. We conclude that intracellular acidification is sufficient to activate taste cells that express PKD2L1 and mediate sour taste, but not taste cells that express TRPM5 and mediate bitter, sweet, and umami taste.

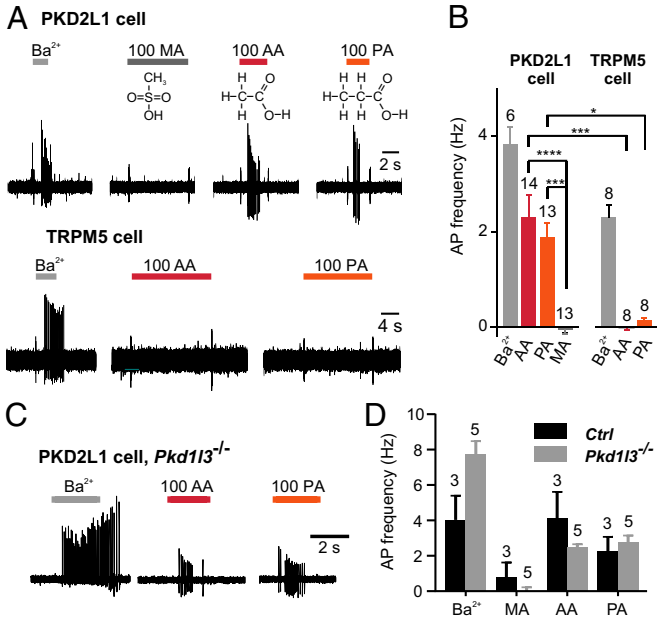

Fig. 1. Intracellular acidification evokes action potentials in dissociated PKD2L1 cells but not TRPM5 cells. (*A*) Action potentials were evoked in a PKD2L1 cell (*Upper*) but not in a TRPM5 cell (*Lower*) in response to 100 mM acetic acid (AA) and propionic acid (PA), adjusted to pH 7.4. Control stimuli were 100 mM methanesulfonic acid (MA), or 2 mM Ba^{2+}. Structural formulae of acids are shown. (*B*) Average data from experiments as in *A*. The numbers of cells tested are indicated above the bars. By one-way ANOVA, there was a significant difference in the response of PKD2L1 cells to AA and PA compared with MA. Asterisks indicate *P* value from Tukey's post hoc test. ***$P < 0.001$, ****$P < 0.0001$. By two-way ANOVA, there was a significant difference in the response to weak acids between cell types ($P < 0.0001$), but no difference between the response to the two weak acids ($P = 0.70$). Asterisks indicate *P* value from Tukey's post hoc test. *$P < 0.05$, ***$P < 0.001$. (*C*) Action potentials evoked in a PKD2L1 cell from CV of a *Pkd1l3*$^{-/-}$ animal in response to 100 mM AA, 100 mM PA, or 2 mM Ba^{2+}. (*D*) Average data from experiments as in *C*. By two-way ANOVA, there was no significant difference in response to acidic stimuli (MA, PA, and AA) across genotypes ($P = 0.37$).

Intracellular Acidification Blocks Resting K^+ Currents in PKD2L1 Cells. Intracellular acidification could generate membrane depolarization either by activating excitatory, Na^+- or Ca^{2+}-permeable, channels, or by inhibiting K^+ channels (3, 28). We previously tested whether weak acids could activate an inward Na^+- or Ca^{2+}-permeable current in PKD2L1 cells and failed to find any difference in the magnitude or reversal potential of the inward current evoked in response to pH 5 with or without acetic acid (16). We also tested whether the channel complex formed from PKD2L1/PKD1L3 contributes to the response to weak acids (29). Cells isolated from *Pkd1l3*$^{-/-}$ animals responded vigorously to 100 mM AA and 100 mM PA (pH 7.4), and no difference in response intensity could be detected between knockout animals and wild-type (WT) littermates (two-way ANOVA, $P = 0.37$; Fig. 1 *C* and *D*). Because PKD1L3 is required for membrane trafficking of the PKD2L1 (9), we conclude that PKD2L1/PKD1L3 does not contribute to the depolarization in response to intracellular acidification.

We next tested whether, instead, cytosolic acidification had an effect on the resting K^+ currents in PKD2L1 cells, measured by elevating extracellular K^+ to 50–140 mM. The inward K^+ current (at −80 mV) was unaffected by lowering the pH of the extracellular solution (to pH 6.0), but was strongly inhibited by 20 mM acetic acid, pH 6.0, a condition that acidifies the cell cytosol (27) (Fig. 2 *A* and *B*). The block by acetic acid developed over tens of seconds and recovered over a similar time course (Fig. 2*A*), as expected if the protonated form of the acid must enter the cell to block the channel.

Identity of the Acid-Sensitive Resting K^+ Current. To identify candidates to mediate the resting K^+ current in PKD2L1 cells, we analyzed the transcriptome of lingual epithelium containing circumvallate papillae and compared it with the transcriptome of nontaste epithelium (NT) (Fig. 2*C*). We focused on inward rectifier channels (K_{IR} family) and two-pore domain K^+ channels (K_{2P}), based on our preliminary results, and known functions of these channels in mediating the resting potential in other cell types. Altogether, we detected moderate-to-high expression of eight K_{IR} channels and five K_{2P} channels in taste tissue (Fig. 2*C*); four additional K_{2P} channels were detected at low levels and were not pursued further. The eight K_{IR} channels ($K_{IR}2.1$, 2.2, 3.1, 3.4, 1.1, 4.2, 6.1, and 6.2) included two that were previously identified in taste cells: $K_{IR}1.1$ (ROMK1), which is expressed by type I taste cells (30), and $K_{IR}6.1$, a component of a K_{ATP} channel, expressed by type II taste cells (31). Among the five K_{2P} channels (Task2, Trek1, Twik1, Twik2, and Twik3), we observed particularly high expression of Twik1 (KCNK1) and lower expression of Task-2, which were previously reported to be expressed in taste tissue (22, 23). As a control, we examined expression of *Pkd2l1* and *Trpm5*; both were highly and specifically expressed in taste tissue, as expected (Fig. 2*C*).

We next used pharmacological profiling to determine which among the 13 K_{IR} and K_{2P} channels mediates the resting K^+ current in PKD2L1 cells. Of the K^+ channel blockers tested (32, 33), the resting K^+ current in PKD2L1 cells was sensitive

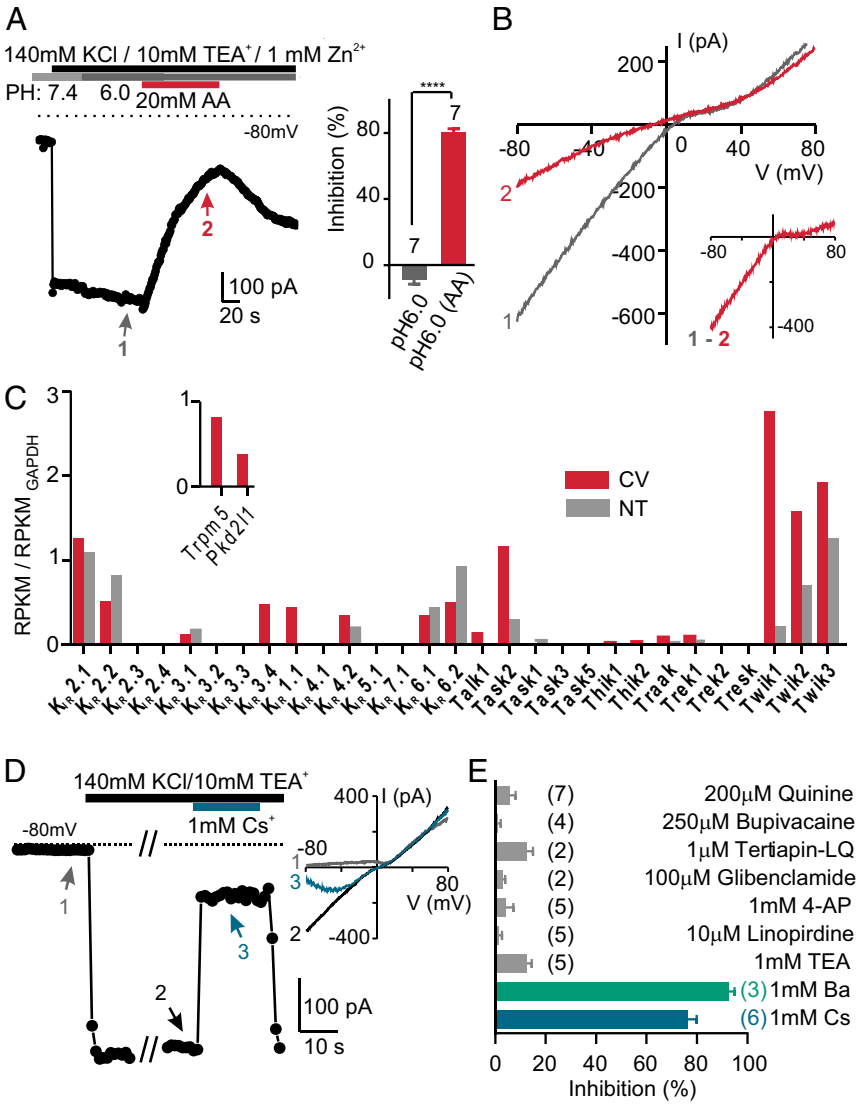

Fig. 2. An inward rectifier K^+ current in PKD2L1 cells is inhibited by intracellular acidification. (*A*) The inward K^+ current measured in a PKD2L1 cell was reversibly inhibited by 20 mM acetic acid, pH 6.0, but not by pH 6.0 alone. Average data are shown in the *Inset*. ****$P < 0.0001$ using paired two-tailed Student's *t* test. (*B*) *I–V* relation measure at the times indicated in *A*. Note that the difference current shows inward rectification. (*C*) The normalized expression levels of Kcnj (K_{IR}) and Kcnk (K_{2P}) transcripts from deep sequencing of taste and nontaste tissues (average of two samples each). The mapped reads were used to compute reads per kilobase per million reads (RPKM) for each gene, which was further normalized to the RPKM of GAPDH in each sample. *Inset* shows expression level of two taste cell markers, *Trpm5* and *Pkd2l1*, which were detected only in taste tissue. (*D*) The inward K^+ current from a PKD2L1 cell was reversibly blocked by 1 mM Cs^+. *Inset* shows *I–V* relation measured at the time points indicated. (*E*) K^+ channel blockers were tested against resting K^+ currents in PKD2L1 cells in 100 mM NaCl, 50 mM KCl. The number of cells tested is indicated next to the bars. Of the compounds tested, only 1 mM Ba^{2+} and 1 mM Cs^+ produced a significant block of the inward K^+ current ($P < 0.0001$ by one-way ANOVA followed by Tukey's post hoc analysis).

only to 1 mM Ba^{2+} and 1 mM Cs^+ (Fig. 2 *D* and *E*; one-way ANOVA, $P < 0.0001$). Notably, the current was insensitive to quinine (Fig. 2*E*), excluding contributions from Twik1-3 (sensitivity to Cs^+ excludes the remaining K_{2P} channels). The current was also insensitive to tertiapin-LQ (targets $K_{IR}1.1$ and $K_{IR}3.1/3.4$), glibenclamide (targets $K_{IR}6.1$ and 6.2), tetraethylammonium (TEA), 4-aminopyridine (4-AP), and linopiridine (target Kv and KCNQ channels) (Fig. 2*E*). Of the channels expressed in taste tissue, only the inward rectifiers $K_{IR}2.1$, $K_{IR}2.2$, and $K_{IR}4.2$ have this pharmacological profile.

To narrow down the candidates further, we assessed the sensitivity of the resting K^+ current in PKD2L1 cells to block by Ba^{2+} and Cs^+ (Fig. 3 *A–D*). Block of the current by Cs^+ was strongly voltage dependent (Figs. 2*D* and 3 *A* and *B*) with an IC_{50} of 211 ± 35 μM measured at −80 mV. A similar sensitivity to Cs^+ was measured for heterologously expressed $K_{IR}2.1$ and 4.2 (IC_{50} values of 169 ± 8 and 194 ± 19 μM, respectively), whereas heterologously expressed $K_{IR}2.2$ showed a significantly higher sensitivity to Cs^+ (118 ± 9; $P < 0.05$ by one-way ANOVA followed by Tukey's multiple-comparison test). Sensitivity to Ba^{2+} was even more informative. Ba^{2+} blocked the K^+ current in PKD2L1 cells with an IC_{50} of 2.1 ± 0.4 μM (measured at −80 mV), which was not significantly different from the IC_{50} for inhibition of $K_{IR}2.1$ (1.4 ± 0.2 μM; Fig. 3 *C* and *D*), but considerably different from the IC_{50} of either $K_{IR}2.2$ or $K_{IR}4.2$ (0.23 ± 0.06 and 5.8 ± 0.8 μM, respectively; $P < 0.0001$ and $P < 0.01$ by one-way ANOVA followed by Tukey's multiple-comparison test). Finally, we tested the $K_{IR}2$-specific blocker ML133, which has a reported IC_{50} of 1.9 μM for $K_{IR}2.1$ (34). ML133 (50 μM) blocked the resting K^+ current in PKD2L1 cells by ∼90%, similar to its effect on $K_{IR}2.1$ and $K_{IR}2.2$, whereas $K_{IR}4.2$ was virtually insensitive to ML133 (Fig. 3 *E* and *F*). Moreover, we observed an increase in the rate of inhibition by ML133 when the pH of the extracellular solution was raised to 8.5, as previously described for $K_{IR}2.1$ (Fig. S2) (34). Thus, based on sensitivity to Ba^{2+}, Cs^+, and ML133, we conclude that the resting K^+ current in PKD2L1 cells is mediated by $K_{IR}2.1$.

Sensitivity to intracellular acidification is not a well-documented feature of $K_{IR}2.1$ as it is for other K_{IR} and K_{2P} channels (35, 36). We therefore tested whether heterologously expressed $K_{IR}2.1$ channels could be blocked by intracellular acidification. Indeed, $K_{IR}2.1$ currents were potently inhibited by 20 mM acetic acid, pH 6, and to a similar degree as currents in PKD2L1 cells (Fig. 4*A*; compare with Fig. 2*A*), but not by extracellular acid alone (Fig. 4 *A–C*). Moreover, in excised patches of cells heterologously expressing $K_{IR}2.1$ channels, we found that exposure of the cytoplasmic surface to acidic pH (pH <6) produced a rapid and partially reversible block of channel activity (Fig. 4*D*).

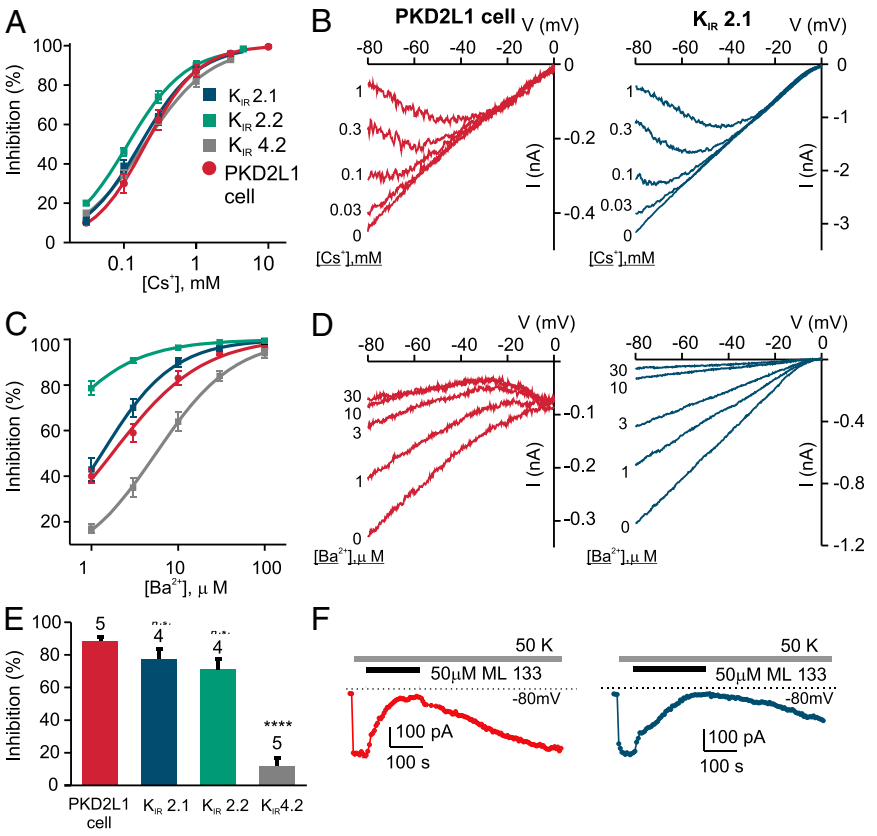

Fig. 3. Pharmacological profile of the resting K^+ current in PKD2L1 cells implicates $K_{IR}2.1$. (*A–D*) The dose dependence of Cs^+ and Ba^{2+} block of inward K^+ currents at –80 mV in PKD2L1 cells compared with that of $K_{IR}2.1$, $K_{IR}2.2$, and $K_{IR}4.2$ expressed in HEK 293 cells (mean ± SEM of four to seven cells). (*A*) By two-way ANOVA, there was a significant difference in sensitivity to Cs^+ block between currents in PKD2L1 cells and HEK cells transfected with the K_{IR} channels ($P < 0.05$). Tukey's post hoc analysis showed significant difference in Cs^+ block between PKD2L1 cells and $K_{IR}2.2$ at a concentration of 30 μM ($P < 0.05$). (*B*) The *I–V* relationships of the inward K^+ current in PKD2L1 cells or HEK cells transfected with $K_{IR}2.1$ measured in the presence of the indicated concentration of Cs^+. V_m was –80 mV, and the voltage was ramped to +80 mV (1 V/s). Note that block is strongly voltage dependent. (*C*) Two-way ANOVA showed a significant difference ($P < 0.0001$) in sensitivity to Ba^{2+} block between currents recorded from PKD2L1 cells and HEK cells transfected with the K_{IR} channels. Tukey's post hoc analysis showed that $K_{IR}2.1$ and PKD2L1 currents differed only in response to 3 μM ($P < 0.01$); at all other concentrations, there was no significant difference. (*D*) *I–V* relationships from experiments as in *C*. (*E*) Percentage block by ML133 (50 μM) of the inward K^+ current in PKD2L1 cells and HEK cells heterologously expressing and K_{IR} channels. By one-way ANOVA, there was a significant difference in ML133 block efficiencies across K^+ channel types ($P < 0.0001$). Asterisks indicate *P* value compared with PKD2L1 cell using Tukey's multiple-comparisons test. ****$P < 0.0001$. (*F*) Representative data showing the time course of the block by ML133 of the inward K^+ current in a PKD2L1 cell and a cell heterologously expressing $K_{IR}2.1$.

Thus, among K^+ channels expressed in taste epithelium, $K_{IR}2.1$, with a pharmacological profile nearly identical to that of the resting K^+ current in PKD2L1 cells, including a similar sensitivity to intracellular acidification, is a strong candidate for mediating the resting K^+ current of PKD2L1 cells.

Tissue-Specific Knockout Confirms the Contribution of $K_{IR}2.1$ to the Resting K^+ Current. To further determine whether $K_{IR}2.1$ accounts for the resting K^+ current in PKD2L1 cells, we measured currents in cells isolated from mice carrying a targeted deletion of the gene. Because knockout of $K_{IR}2.1$ is neonatal lethal (37) and it is difficult to identify sour taste cells by expression of YFP at birth, we chose to use a tissue-specific gene deletion strategy. To this end, we used a mouse strain carrying a floxed allele of *Kcnj2* (*Methods*) and crossed it to a mouse strain in which the *Pkd2l1* promoter drives expression of Cre recombinase. Based on use of a floxed Tdt reporter, Cre is expected to be active in ~79% of the *Pkd2l1*-expressing cells, and only in *Pkd2l1*-expressing cells in the circumvallate papillae (Fig. 5*A* and Fig. S3). We confirmed that *Kcnj2* was inactivated in taste tissue using a PCR strategy designed to detect the deletion event (Fig. S4).

The resting K^+ current in animals carrying two floxed alleles of *Kcnj2* and one allele of *Pkd2l1*-Cre (cKO) was compared with that in littermates that carried either the floxed allele or the *Pkd2l1*-Cre driver alone. As shown in Fig. 5 *B–D*, the average magnitude of the resting K^+ current in the cKO animals was significantly reduced compared with either control group (one-way ANOVA followed by Tukey's post hoc test, $P < 0.001$ compared with Cre^+ and $P < 0.01$ compared with $Kcnj2^{fl/fl}$). We also measured sensitivity of the current to 1 μM Ba^{2+}, a concentration that is expected to produce ~50% block of $K_{IR}2.1$. Ba^{2+} produced a substantial (>15%) block of the inward K^+ current in all cells isolated from WT mice (18 of 18), whereas in a significant proportion cells from the cKO, the inward current was Ba^{2+}-insensitive (4 of 18; $P < 0.05$ by one-tailed χ^2 test; Fig. 5*E*). These cells tended to be the ones with the smallest inward current, and thus likely represent cases where the *Kcnj2* gene was completely excised and the $K_{IR}2.1$ protein eliminated. In the remaining cells, the observation that the residual current retained sensitivity to Ba^{2+} indicates that it is not a product of a compensatory increase in the expression of a different subtype of ion channel, but instead likely represents incomplete elimination of the *Kcnj2* gene product. Thus, tissue-specific knockout of *Kcnj2* significantly reduces the magnitude of the resting K^+ current in PKD2L1 cells and eliminates the current in a subset of cells, lending support to the conclusion that $K_{IR}2.1$ mediates this current.

The Magnitude of the K^+ Current Determines Sensitivity to Weak Acids. These data argue that, in response to weak acids, inhibition of $K_{IR}2.1$ by intracellular acidification produces membrane depolarization that drives action potentials in PKD2L1 cells. To directly test this hypothesis would require replacing $K_{IR}2.1$ with an acid-insensitive variant, which is not currently possible. Instead, we reasoned that there should be a correlation between sensitivity to weak acids and expression of $K_{IR}2.1$, such that a cell that is insensitive to weak acids should not express $K_{IR}2.1$ or a similar acid-sensitive K^+ channel. TRPM5 taste cells are insensitive to weak acids (Fig. 1), and we therefore measured the resting K^+ current in these cells. To our surprise, we found that the resting K^+ current in TRPM5 cells was inhibited by exposure to weak acids (Fig. 6*A*), to a similar extent to that of the current in PKD2L1 cells. Moreover, among known blockers of K^+ channels tested, the resting K^+ current in TRPM5 cells was sensitive to only Cs^+ and Ba^{2+}, like the resting K^+ current PKD2L1 cells (Fig. 6*B*; compare with Fig. 2*A*), indicating that it is likely mediated by $K_{IR}2.1$. To directly test this hypothesis, we

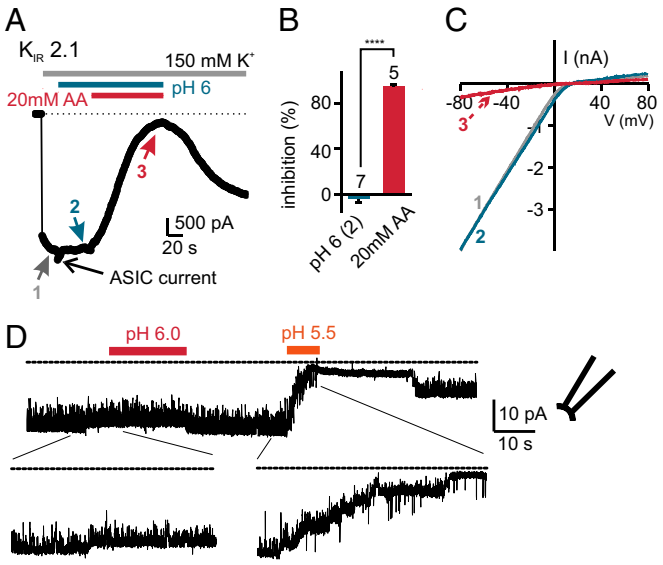

Fig. 4. K_{IR}2.1 is inhibited by intracellular acidification. (*A*) The current in a HEK cell heterologously expressing K_{IR}2.1 is inhibited by 20 mM acetic acid at pH 6, but not by pH 6 alone. Note that the pH 6 solution evokes an inward current carried by acid-sensing ion channels (ASIC). (*B*) Average data from seven cells as in *A* normalized against the current magnitude before the application of acid. ****$P < 0.0001$ using paired two-tailed Student's *t* test. (*C*) The *I–V* relationship of the K_{IR}2.1 current at times indicated in *A*. (*D*) Excised patch recording from a K_{IR}2.1 transfected HEK cell in response to acids. The bath solution contained 150 mM KCl, 1 mM EGTA, and 1 mM EDTA. The membrane was held at −80 mV. The application of pH 5.5 completely inhibited channel activity, and channel activity was partially restored by return to neutral pH. Similar results were observed in five cells.

generated a cell type-specific knockout of *Kcnj2*, this time using the *Advillin* promoter (38), which drove expression of Cre in ∼71% of TRPM5 cells (Fig. 7*A* and Fig. S5). We then measured the resting K^+ current in cKO and control cells (Fig. 7 *B* and *C*). Although there was no change in the average magnitude of the current (Fig. 7*D*), the Ba^{2+}-sensitive resting K^+ current was eliminated in a subpopulation of cKO cells (5 of 24) but not in any control cells (0 of 13; $P < 0.05$; one-tailed χ^2 test) (Fig. 7*E*). This supports the interpretation that K_{IR}2.1 contributes to the resting K^+ current in TRPM5 cells.

We next determined whether TRPM5 cells and PKD2L1 cells acidified to the same extent in response to the weak acid stimuli. Freshly isolated cells were loaded with the pH-sensitive dye phrodo red, and fluorescent intensity was monitored under the same conditions used to measure action potentials in cell-attached recording. As we previously reported, PKD2L1 cells had an initial starting pH that was acidified compared with that of TRPM5, a phenomenon that can be attributed to proton leak through ungated proton channels in these cells (21). There was, however, no difference in the final pH reached in response to the weak acid solutions between cell types (pH 6.47 ± 0.08 in TRPM5 cells versus 6.34 ± 0.05 in PKD2L1 cells, $P = 0.43$ by two-way ANOVA followed by Sidak's multiple-comparison test; Fig. S6).

Thus, TRPM5 cells express a resting K^+ channel sensitive to intracellular pH and show a drop in intracellular pH in response to weak acids, similar to that in PKD2L1 cells. Why then do they not fire action potentials to weak acids? In contemplating this question, we noticed that there was one important difference between the resting K^+ currents in PKD2L1 and TRPM5 cells—the K^+ currents were severalfold larger in TRPM5 cells compared with PKD2L1 cells (Fig. 8 *A* and *B*). The larger K^+ current is expected to more effectively clamp the resting potential of TRPM5 cells, reducing sensitivity to K^+ channel blockers such as intracellular acidification. To test this hypothesis, we used a low concentration of Ba^{2+} (10 μM) to reduce the magnitude of the resting K^+ current in the TRPM5 cells to the level observed in PKD2L1 cells (Fig. 8 *A* and *B*). We then asked whether under these conditions TRPM5 cells would fire action potentials to weak acids. Indeed, when primed with 10 μM Ba^{2+}, which alone did not stimulate action potentials, the TRPM5 cells fired action potentials to weak acid stimulation (Fig. 8 *C* and *D*). These data are consistent with the hypothesis that the acid-sensitive K_{IR}2.1 channels mediate responses to weak acids in PKD2L1 cells; the small magnitude of this current, relative to other conductances, and not its identity, restricts acid sensitivity to these cells.

The Resting K^+ Current Is Blocked Downstream of H^+ Entry Through a Zn^{2+}-Sensitive Conductance. The pH sensitivity of K_{IR}2.1 makes it well suited to be part of the sour transduction machinery, acting to transduce cellular acidification into a change in membrane potential. Intracellular acidification can be elicited in PKD2L1 cells when protons enter through an apical conductance. In the previous experiments, we took safeguards to prevent proton entry through the proton conductance, which would have generated an increase in the inward current and confounded interpretation of the results. Thus, whenever the extracellular solution was acidified, we added Zn^{2+} (2 mM) to block the proton current (16, 21). To determine whether entry of protons through the proton conductance could block the resting K^+ current in PKD2L1 cells, we simply measured the response to extracellular acidification in the absence of Zn^{2+}. As seen in Fig. 9 *A* and *B*, the resting K^+ current was inhibited when the pH of the extracellular solution was lowered to 6.0 in the absence of Zn^{2+} (48 ± 7% at 120 s), but not in its presence (13 ± 5%). A similar block of the K^+ current in TRPM5 cells was not observed (Fig. 9*A*), consistent with the observation that these cells do not have a proton current (16, 21).

These data suggest that there are two components to the sensory response to sour stimuli: H^+ entry through a proton channel and intracellular acidification, which blocks resting K^+ channels. To determine whether the two components act synergistically, we tested the response to two subthreshold stimuli: mild extracellular acidification (pH 7.0) and a low concentration of acetic acid (0.1 mM of protonated acid; *Methods*) either alone or in combination. Neither alone was sufficient to stimulate action potentials, but together they strongly activated PKD2L1 cells (Fig. 9 *C* and *D*). At more acidic pH (6.6), action potentials were evoked even in the absence of the weak acid as we previously reported (21), and addition of the weak acid did not produce a significant change in firing rate.

Together, these results suggest that protons serve not only as charge carriers to generate membrane depolarization but also as second messengers that amplify the primary sensory response (Fig. 10).

Discussion

Based on the observation that many of the most potent sour stimuli are weak acids, it has long been speculated that intracellular acidification plays an important role in the transduction of sour taste (5, 19, 39). Consistent with this possibility, here we show for the first time (to our knowledge) that intracellular acidification alone, in the absence of extracellular acidification, can excite sour taste cells. We identify the mechanism by which intracellular acidification excites sour taste cells, as block of a resting K^+ current, whose molecular identity we reveal to be K_{IR}2.1. Surprisingly, K_{IR}2.1 is not specifically expressed by sour taste cells, and thus sensitivity to acids is not conferred by the expression of the channel alone. Instead, we find that sensitivity to weak acids can be attributed to the small magnitude of the current in the PKD2L1 cells compared with

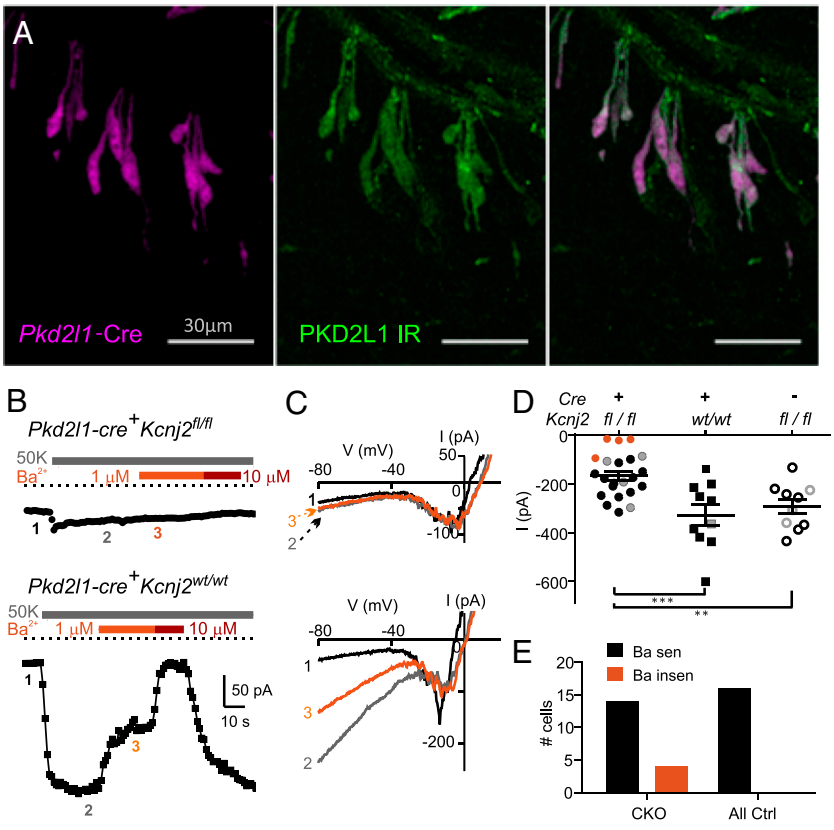

Fig. 5. Tissue-specific knockout of *Kcnj2* in PKD2L1 taste cells confirms that $K_{IR}2.1$ contributes to the inward K^+ current. (*A*) Confocal image of circumvallate taste buds from a *Pkd2l1*-Cre::*Rosa26*^{tdT} mouse. Tomato reporter expression is displayed in magenta. PKD2L1 immunoreactivity is displayed in green. Cre expression efficiency, as determined by the tomato reporter fluorescence, is ~79% in circumvallate taste tissue. (All scale bars: 30 μm.) (*B*) A representative recording from a PKD2L1 cell from a *Pkd2l1*-Cre::*Pkd2l1*-YFP::*Kcnj2*$^{fl/fl}$ mouse (cKO; *Upper*) and a recording from a control cell, from a mouse where *Kcnj2* is not floxed (*Lower*). In the cKO, the K^+ current induced by 50 mM K^+ is small, and not sensitive to 1 or 10 μM Ba^{2+}. (*C*) The *I–V* curves at indicated time points in *B*. (*D*) K^+ current magnitudes in PKD2L1 taste cells from cKO mice and controls. Black symbols indicate the current was sensitive to 1 μM Ba^{2+} (>15% block); red indicates not sensitive (<5% block); gray are cells not tested with Ba^{2+}. One-way ANOVA followed by Tukey's post hoc test, $^{**}P < 0.01$, $^{***}P < 0.001$. (*E*) Same data as in *D* showing the distribution of Ba^{2+}-sensitive currents across genotypes. The difference is significant by one-tailed χ^2 test ($P < 0.05$).

cells that are acid insensitive, such as taste cells responsive to bitter/sweet and umami (TRPM5 cells). Finally, we show that block of the resting K^+ current can also be elicited by elevation of protons following entry through a Zn^{2+}-sensitive conductance, which is the first step in the transduction of strong acids (16). This provides a mechanism for amplification of the sensory response. This mechanism is very different from a recently proposed mechanism for detection of acids by chemosensory neurons in the retrotrapezoid nucleus, which use a proton-activated receptor, GPR4, in combination with a K2P channel sensitive to extracellular pH (TASK-2) (40).

Acid-Sensitive Resting K Current Is Mediated by $K_{IR}2.1$, Not KCNK1. Block of K^+ channels that are open at the resting membrane potential (resting K^+ channels) has previously been suggested as a potential mechanism for sour transduction, although the specific elements of such a pathway have been uncertain. Using the mudpuppy, it was found that extracellular protons block apically located K^+ channels (41, 42), but this mechanism does not appear to apply to other more conventional model systems. More recently, K^+ (K_{2P}) channels, which are sensitive to either intracellular or extracellular protons and thus are well suited to play a role in sour transduction were identified in rodent taste cells (22, 23). However, although electrophysiological properties of each type of taste cell have been described (43, 44), before our study, very little was known about the molecular nature of the K^+ channels that set the resting potential in taste cells and their sensitivity to intracellular or extracellular acidification.

Our data show that there is an acid-sensitive resting K^+ current in sour cells, but that this current is not mediated by the K_{2P} channel Twik1/KCNK1 (22, 23). Although we found that KCNK1 was expressed at significantly higher levels than other K_{2P} or K_{IR} channels, we were unable to detect a current with the pharmacological profile of KCNK1. We calculate that KCNK1 contributes no more than 1% to the resting K^+ current (Fig. S7).

Instead, pharmacological and molecular profiling indicate that $K_{IR}2.1$ channels mediate the resting, acid-sensitive K^+ current in sour taste cells. This is supported by the observation that the resting K^+ currents in PKD2L1 cells from a tissue-specific $K_{IR}2.1$ KO mouse are significantly reduced in magnitude, and in a subset of PKD2L1 cells, the K^+ current is completely eliminated. We did not expect to observe a complete elimination of the current in all cells because a reporter for the driver showed activity in only 70% of PKD2L1 cells. The same argument applies to TRPM5 cells, where the promoter that we used to drive expression of Cre, is effective at most in ~70% of cells and fewer if one considers only cells that show strong expression of the reporter (~50%). Moreover because the *Pkd2l1* Cre driver is expressed by mature neurons, it is only expected to excise the floxed allele at a time when there may already be significant expression of ion channels; under these circumstances, elimination of the current would only be observed if the existing protein has turned over and both alleles of *Kcnj2* were inactivated. Given the short lifetime of taste cells (~22 d) (45), the likelihood that all these events occur before a cell dies is low. Nonetheless, the significant reduction in the resting K^+ current in the tissue-specific KO mice, together with our pharmacological and expression profiling data, provide strong evidence that $K_{IR}2.1$ is required for the resting K^+ current in sour taste cells.

$K_{IR}2.1$ is an unexpected player in sour taste transduction, as the channel was not previously known to be expressed in taste cells or to be associated with sensitivity to intracellular acidification. Notably, $K_{IR}2.1$ is much less sensitive to intracellular acidification than other inward rectifiers, such as $K_{IR}2.3$ and $K_{IR}1.1$ (35). Nonetheless, $K_{IR}2.1$ can be inhibited at a sufficiently low intracellular pH (≤5.5; our data and ref. 35). Moreover, we find that $K_{IR}2.1$ can be blocked in whole-cell recording by weak acids that activate sour taste cells. Under these conditions, the block is slow because the concentration of the protonated form of the weak acid is low, and protons can diffuse out

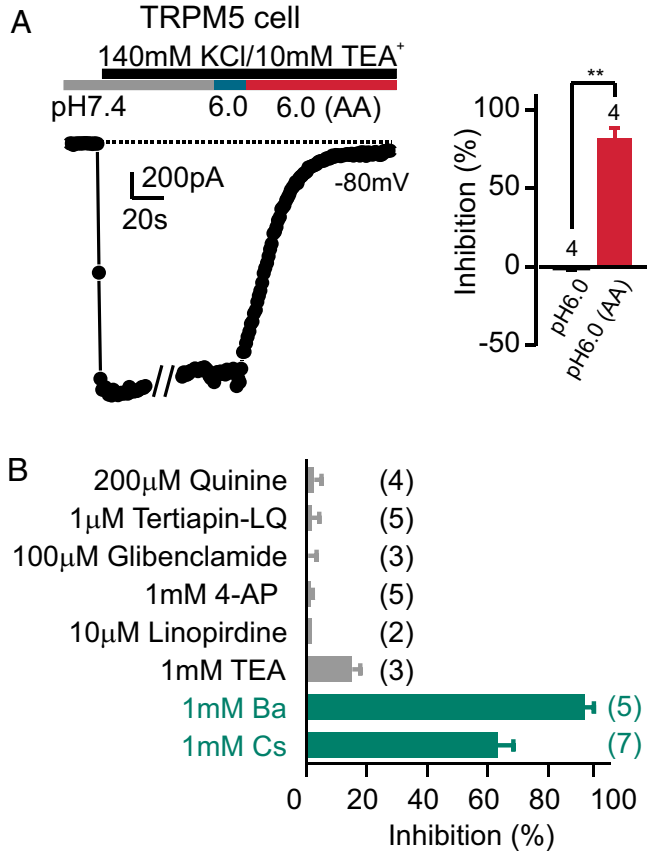

Fig. 6. The resting K^+ current in TRPM5 cells is sensitive to intracellular acidification. (*A*) Inward K^+ currents measured at −80 mV from a TRPM5 cell are sensitive to intracellular acidification (pH 6.0 solution containing 20 mM acetic acid) but not extracellular acidification (6.0 solution buffered with 10 mM Mes). Average data are shown in the right panel. $^{**}P < 0.01$ using paired two-tailed Student's *t* test. (*B*) The pharmacological profiling of the resting K^+ current in TRPM5 taste cells. The inhibition efficiency was tested in 50 mM K^+ solutions at −80 mV as for the PKD2L1 cells. Of the blockers tested, only 1 mM Ba^{2+} and 1 mM Cs^+ produced a significant block of the inward K^+ current ($P < 0.0001$ by one-way ANOVA followed by Tukey's post hoc analysis).

of the cell and into the pipette. We speculate that the reduced sensitivity of $K_{IR}2.1$ to intracellular pH may be advantageous in the context of the sour taste cell, which is acidified at rest (21). Indeed, we do not know the extent of intracellular acidification that occurs in intact taste cells during sensory stimulation, but assuming that proton entry occurs through channels located on sensory microvilli, it is likely that local concentrations of protons could be very high (46). Under these conditions, a less sensitive channel, like $K_{IR}2.1$, would be better able to sense dynamic changes in intracellular pH.

The Magnitude of the Current, and Not the Identity, Determines Sensitivity to Acids. Our experiments show that, among taste cells, only those that mediate sour taste respond to intracellular acidification with action potentials. However, quite unexpectedly this response cannot be attributed to the expression of a highly specialized ion channel whose distribution is restricted to sour taste cells. Instead, sensitivity to intracellular acidification is conferred by a relatively ubiquitous ion channel, $K_{IR}2.1$. $K_{IR}2.1$ (IRK1/KCNJ2) was the first member of the family of inward rectifier ion channels to be identified (47), and it is expressed broadly in the brain, heart, vascular smooth muscle cells, skeletal muscle, and throughout the body (47). Our data also indicate that $K_{IR}2.1$ mediates the resting K^+ current in TRPM5 cells, which are unresponsive to weak acids that stimulate action potentials in PKD2L1 cells. In an attempt to reconcile these findings, we found one way in which the resting K^+ currents in TRPM5 and PKD2L1 cells differed substantially—in their magnitude. As previously reported (44), the resting K^+ currents in TRPM5 cells are severalfold larger than those of PKD2L1 cells. This difference in the magnitude of the K^+ current can completely account for the difference in sensitivity to intracellular acidification between the two cells types as inhibition of the K^+ currents in TRPM5 cells to the level observed in PKD2L1 cells rendered the TRPM5 cells responsive to intracellular acidification. Thus, a smaller K^+ current, as found in PKD2L1 cells, makes the cells more responsive to intracellular acidification.

To gain a quantitative appreciation of this phenomenon, we consider two hypothetical cells that vary only in the magnitude of their resting K^+ current. The first cell (representing the PKD2L1 cell) has a mixed cation conductance of 0.25 nS and a resting K^+ conductance of 1 nS. A resting potential of −67 mV is calculated from the equation: $V_m = [(G_K{*}E_K) + (G_C{*}E_C)]/(G_K + G_C)$, where G_K and E_K are the K^+ conductance and equilibrium potential, G_C and E_C are the cation conductance and cation equilibrium potential, and the K^+ concentration is assumed to be 5 mM outside the cell and 140 mM inside it (48). The same equation can be used to show that it would be necessary to block 60% of the K^+ current to reach threshold for firing action potentials (assumed to be −50 mV). Now consider another cell (a TRPM5 cell), with a similar resting cation conductance, but a threefold larger K^+ conductance (3 nS). The resting potential of this cell is calculated to be −77 mV. Block of 50% of the current will depolarize the cell to −72 mV. In this cell, it is necessary to block 87% of the current to depolarize the cell to a threshold of −50 mV. Thus, one can see that, in moving from a cell with a small resting K^+ current to one with a larger current, the fractional block of the current required to reach threshold has increased substantially, from 60% to 87%. If one further assumes a single-site binding site model for block of the channel, this translates into a need for a ∼4.5-fold higher concentration of intracellular protons to bring the TRPM5 cell to threshold compared with the PKD2L1 cell (*Methods*). Thus, without considering other conductances, the smaller K^+ current in PKD2L1 cells is expected to make the cells much more sensitive to intracellular acidification compared with TRPM5 cells.

It is also worth noting that, among a variety of cells tested, only PKD2L1 cells have an inward proton conductance, which can act upstream of the acid-sensitive K^+ channel (21). Thus, in other cells in the taste bud, the only way that the cytosol can be acidified is by penetration of weak acids. Although these factors make it unlikely that in vivo TRPM5 taste cells will fire action potentials to acids, we cannot rule out the possibility that intracellular acidification might modulate the response of TRPM5 cells to bitter, sweet, and umami stimuli. Moreover, because we looked only at the aggregate behavior of TRPM5 cells, it is possible that a small subset of TRPM5 cells responsive to one taste quality could show heightened sensitivity to intracellular acidification, and possibly even fire action potentials under some conditions.

Does This Explain the Sour Taste of Weak Acids? It was noted nearly a century ago that at the same pH, organic weak acids evoke a more intense sour sensation than strong mineral acids (18). This has been attributed to the ability of weak acids, in the protonated form, to penetrate the cell membrane, and upon entering the cell, release a proton (28). Cytosolic acidification could then affect membrane excitability and/or transmitter release. Consistent with this hypothesis, a previous study found that the gustatory nerve response was better correlated with the ability of sour stimuli to acidify the cytosol, rather than the absolute concentration of free protons they contained (5). Similar results were found in recordings from a slice preparation of lingual epithelium,

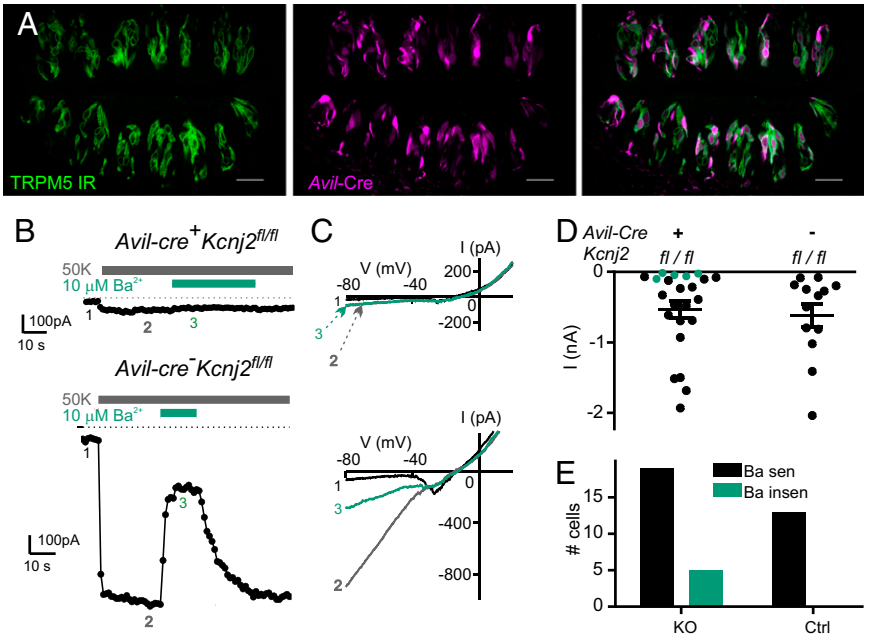

Fig. 7. Tissue-specific knockout of *Kcnj2* in TRPM5 taste cells. (*A*) Confocal image of circumvallate taste buds from an *Avil*-Cre::*Rosa26*^{tdT}::*Pkd2l1*-YFP mouse. Tomato reporter expression is displayed in magenta. TRPM5 immunoreactivity is displayed in green. Cre is expressed in ~71% of TRPM5 cells as determined by expression of the tomato reporter fluorescence in TRPM5-immunoreactive cells. (Scale bar: 30 μm.) (*B*) A representative PKD2L1 cell from a *Avil*-Cre::*Trpm5*-GFP::*Kcnj2*$^{fl/fl}$ mouse (cKO; *Upper*) and a *Cre*$^{-}$ control cell. In the taste cell from the cKO mouse, the K^+ current is small, and insensitive to 10 μM Ba^{2+}. (*C*) *I–V* curves at time points indicated in *B*. (*D*) Magnitude of the K^+ current in TRPM5 taste cells from cKO mice and WT controls. Black symbols indicate the current was sensitive to 10 μM Ba^{2+} (>40% block); green indicates that the current was not sensitive (<25% block). (*E*) Same data as in *D* showing the distribution of Ba^{2+}-sensitive currents across genotypes ($P < 0.05$; one-tailed χ^2 test).

where focal application of sour stimuli elicited calcium responses in taste cells that correlated with the degree of intracellular acidification (20) To our knowledge, our experiments are the first to directly show that intracellular acidification alone, in the absence of extracellular acidification, increases cellular excitability in identified sour taste cells. For these experiments, we used two organic weak acids, acetic acid and propionic acid, which due to their small size and relatively high pK_a values (4.76 and 4.88, respectively) can acidify the cell cytosol when used at neutral pH (27). Application of these acids at neutral pH caused a similar degree of intracellular acidification in both TRPM5 and PKD2L1 cells, but only PKD2L1 cells fired action potentials. However, it is worth noting that, in the intact epithelium where taste buds are surrounded by a relatively impenetrable barrier, weak acids may not enter taste cells unimpeded (49). Alternatively, weak acids may be effective sour stimuli because they buffer pH, protecting protons from absorption by salivary proteins. The extent to which penetration of weak acids into taste cells and the buffering capacity of weak acids contributes to the intensity of sour taste perception remains to be determined.

Role of K_{IR}2.1 in Amplification of the Sensory Response. The ability of K_{IR}2.1 to respond to an elevation of protons makes it well suited to participate in sour transduction, downstream of the previously characterized Zn^{2+}-sensitive proton conductance (Fig. 10). Indeed, we find that the K_{IR}2.1 current in sour taste cells can be blocked by extracellular acidification, when protons are allowed to enter the cell through the Zn^{2+}- sensitive conductance. Block of resting K^+ channels would reduce the extent of proton entry needed to depolarize the sour taste cell to threshold, and thereby enhance the detection of small signals. This may explain how taste cells can respond to bath acidification as mild as pH 6.7, which produces a proton current of only a few picoamperes (21). Moreover, it is possible that K_{IR}2.1 channels are localized in close proximity to proton channels, facilitating interaction between the two molecules.

Amplification is a common theme in sensory biology and is usually associated with signaling by G-protein–coupled receptors that activate a cascade of intracellular events (50, 51). Our proposed mechanism, on the other hand, is most similar to the mechanism of amplification observed in the olfactory system where calcium entering through cyclic-nucleotide gated ion channels acts on chloride channels, which further depolarize the cell membrane (52, 53). This mechanism allows the cell to respond to odorants under circumstances where extracellular ions are limited. Similarly, the use of an intracellular amplification step for sour taste transduction is expected to enhance signaling while limiting the need for excessive proton entry that might be cytotoxic.

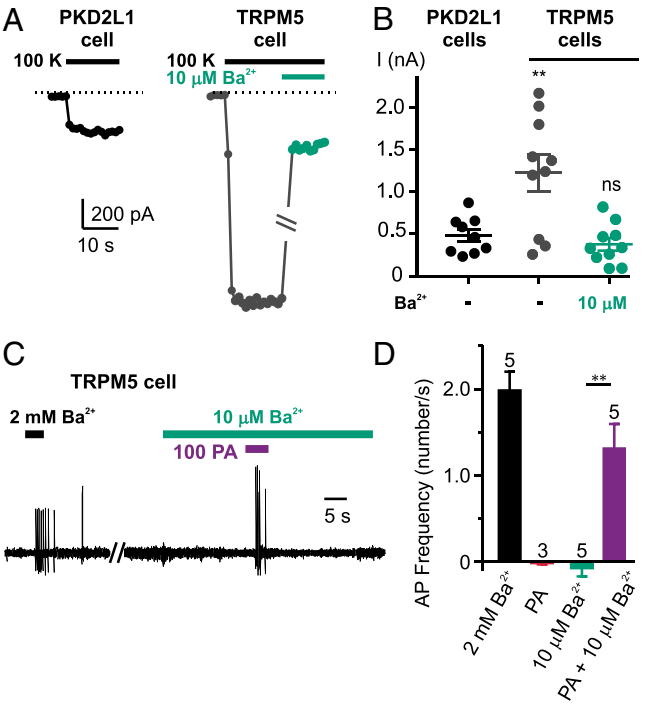

Fig. 8. Reduction in the magnitude of the resting K^+ currents makes TRPM5 cells sensitive to intracellular acidification. (*A*) K^+ (100 mM) elicits significantly larger currents in TRPM5 cells than in PKD2L1 cells and that 10 μM Ba^{2+} reduces the current to a similar magnitude as in PKD2L1 cells. (*B*) Scatter plot of current magnitudes from cells as shown in *A*. Tests for significant difference of TRM5 cells with or without Ba^{2+} were against PKD2L1 cells. $^{**}P < 0.01$ using two-tailed Student's *t* test. (*C*) With the preapplication of 10 μM Ba^{2+}, robust action potentials were elicited by 100 mM propionic acid at pH 7.4. (*D*) The average data of cells as in *C*. $^{**}P < 0.01$ using paired one-tailed Student's *t* test.

Taken together, our experiments provide evidence for the participation of the inward rectifier K^+ channel, $K_{IR}2.1$, as a key element in sour taste transduction. Notably, we find that $K_{IR}2.1$ is blocked by intracellular acidification and acts downstream of proton channels to enhance electrical excitability. Working in tandem, the proton conductance and $K_{IR}2.1$ channel constitute an elegant mechanism for amplification of the sensory response to sour stimuli.

Methods

Animals. All methods of mouse handling were approved by the University of Southern California Institutional Animal Care and Use Committee. Mouse strains *Pkd2l1*-YFP, *Pkd1l3*$^{-/-}$ were previously described (14, 16). Mouse strains *Kcnj2*$^{fl/fl}$, *Pkd2l1*-Cre are described in *SI Methods*. *Avil*-Cre mice were a kind gift from the Peter Heppenstall Laboratory, European Molecular Biology Laboratory, Monterotondo, Rome (38).

Taste Cell Isolation. Taste cells were isolated from adult mice (6–10 wk old) as previously described (16, 21). In brief, Tyrode's solution containing 1 mg/mL elastase (Worthington), 2.5 mg/mL dispase II (Roche), and 1 mg/mL trypsin inhibitor (Sigma-Aldrich) was injected between the epithelium and the muscle of the isolated tongue, which was incubated for 20 min in Tyrode's solution bubbled with 95% O_2/5% CO_2. The epithelium was then peeled off from the tongue. The small piece of epithelium containing the papillae was further trimmed and incubated in the enzyme mixture for 20 min at room temperature. The reaction was stopped by washing the tissue in Ca^{2+}-free saline. Single cells were isolated by trituration in Tyrode's solution with a fire-polished Pasteur pipette and were used within 6 h.

Taste Cell Recording. Taste cells were prepared for patch-clamp recording as previously described (16, 21). Data were collected with an Axopatch 200B amplifier using pClamp software suite (Axon Instruments), and time course measurements and *I–V* curve were graphed with Origin 6 (OriginLab). For cell-attached recording, we selected for cells that were healthy and able to fire action potentials, using 2 mM Ba^{2+}, which elicited action potentials more reliably in both PKD2L1 and TRPM5 cells compared with high K^+ (16). In addition, we selected for cells with intact apical processes, based on the flask-like shape of the cell, and presence of apically located YFP. Firing rates were measured within the interval of 0.4 to 4 s following application of stimuli unless otherwise stated. The evoked frequency was calculated after subtraction of the background frequency, measured during the 10 s before application of the stimulus. Note that the amplitude of the spikes measured in a single cell varied during recordings; this can be attributed to changes in the availability of Na^+ channels, which may not fully recover from inactivation when resting K^+ channels are blocked to changes in the seal resistance, which can affect spike amplitude. For whole-cell recording, the membrane potential was held at –80 mV, the voltage was ramped from –80 to +80 mV (1 V/s), and the current was measured at –80 mV. For testing the dose dependence of inhibition by Ba^{2+} and Cs^+ of the resting K^+ current (Fig. 3 *A–D*), series resistance compensation was performed.

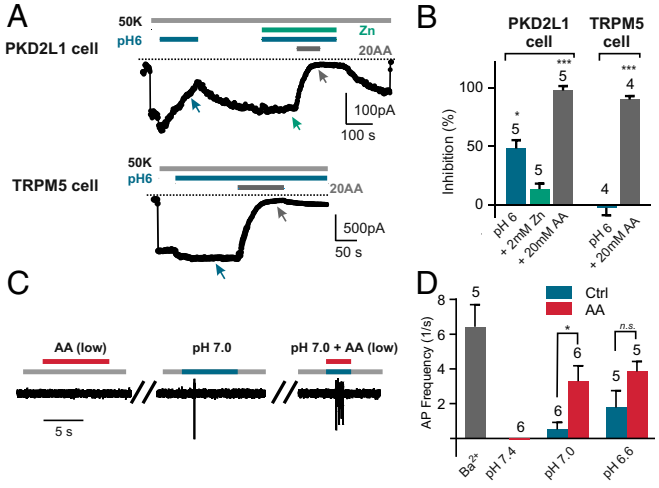

Fig. 9. Block of the resting K^+ current by proton entry through a proton conductance provides a mechanism for amplification of the sour sensory response. (*A*) The inward K^+ current in a PKD2L1 cell, but not a TRPM5 cell, was inhibited by extracellular solution adjusted to pH 6 when 2 mM Zn^{2+}, a blocker of the taste cell proton conductance, was omitted from the solution, but not when it was included. (*B*) Average data from experiments as in *A* at time points indicated by the arrows, normalized against the current magnitude before the application of the pH 6 solution. Asterisks indicate the significant difference compared with pH 6 plus 2 mM Zn^{2+} in PKD2L1 cells, or pH 6 alone in TRPM5 cells. (*C*) Action potential recorded in cell-attached mode from a PKD2L1 taste cell in response to the indicated stimuli. Neither the pH 7.0 stimulus nor a low concentration of AA (0.1 mM of protonated acid) could effectively evoke action potentials, but together they elicited robust firing. (*D*) Average data from experiments as in *C*. By two-way ANOVA, there was a significant difference between Ctrl and AA groups ($P < 0.01$). Asterisks indicate results of Sidak's multiple-comparison test. $*P < 0.05$, $***P < 0.001$.

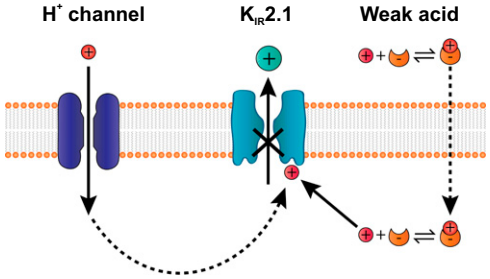

Fig. 10. A two-component mechanism for sour taste transduction. In the proposed model, H^+ entering through an H^+ channel inhibits the K^+ channel. The K^+ channel can also be inhibited by H^+ that is shuttled by weak acids. Both the proton entry and the block of the K^+ channel contribute to membrane depolarization, which drives action potentials and release of neurotransmitter.

Solutions. Solutions for electrophysiology were exchanged using a piezo-driven stepper motor system (SF-77B; Warner Instruments). The pipette solution in all experiments except those shown in Figs. 2*A*, 4*A*, 6*A*, and 9*A* contained the following (in mM): 120 KAsp, 7 KCl, 8 NaCl, 10 Hepes, 2 MgATP, 0.3 GTP-Tris, 5 EGTA, 2.4 $CaCl_2$ (~100 nM free Ca^{2+}), pH 7.4 with KOH. For the experiments shown in Figs. 2*A*, 4*A*, and 6*A*, to minimize contributions due to changes in intracellular Ca^{2+} as a result of competition between H^+ and Ca^{2+} for binding to EGTA, a Ca^{2+}-free pipette solution was used containing the following (in mM): 120 KAsp, 20 KCl, 10 Hepes, 2 MgATP, 0.3 GTP-Tris, 0.5 EGTA, pH 7.3; in Fig. 9*A*, Hepes concentration was 10 μM. Tyrode's solution contained the following (in mM): 140 NaCl, 5 KCl, 2 $CaCl_2$, 1 $MgCl_2$, 10 Hepes, and 10 D-glucose, pH 7.4. Sodium solution was as follows (in mM): 150 NaCl, 10 Hepes, and 2 $CaCl_2$, pH 7.4. For recording action potentials, the tested solutions contained the indicated concentration of acid (in mM), which replaced equimolar Cl^-, and the pH was adjusted with NaOH. In Fig. 9 *C* and *D*, the pH 7.4, pH 7.0, and pH 6.6 solutions have 43.7, 17.5, and 7 mM overall acetic acid, respectively, to generate a final concentration of 0.1 mM protonated form. For whole-cell recordings, 50 mM KCl (Figs. 2*E*, 3 *E* and *F*, 5, 6*B*, 7, 9 *A* and *B*), 100 mM KCl (Fig. 3 *A–D* and 8 *A* and *B*), or 140 mM KCl (Figs. 2 *A* and *D*, and 6*A*) and labeled concentrations of TEA replaced equimolar NaCl in the extracellular solution. For solutions of pH ≤6.6, Mes replaced Hepes. In excised patch, the pipette solution was as follows (in mM): 150 KCl, 2 $CaCl_2$, 10 Hepes, pH 7.4. The extracellular solution was 150 KCl, 10 Hepes or 10 Mes, 1 EDTA, 1 EGTA, pH 7.4 with KOH or HCl.

Chemicals. Glibenclamide and Tertiapin-LQ, bupivacaine, and linopirdine were purchased from Tocris; ML133 was a gift of Craig Lindsley, Vanderbilt University, Nashville, TN. All other chemicals used for pharmacological profiling were from Sigma-Aldrich.

Statistics and Analysis. Bar and summary scatter plots were prepared in Prism (GraphPad Software). Significance was determined with Student's *t* test or ANOVA as indicated. In all cases, data represent the mean ± SEM, $*P < 0.05$, $**P < 0.01$, $***P < 0.001$, $****P < 0.0001$.

Heterologous expression, mouse genetics, immunocytochemistry, transcriptome analysis, intracellular pH imaging, and other experimental details are described in *SI Methods*.

ACKNOWLEDGMENTS. This work was supported by National Institute of Deafness and Communications Disorders (NIDCD) Grants R21 DC012747 and R01 DC013741 (to E.R.L.); NIDCD Grant F32 DC013971-01 (to J.D.B.); NIDCD

Grant R01 DC012555 (to S.C.K.); and NIDDKD Grant R37 DK-053832, NHLBI Grants R01 HL044455, HL121706, and P01 HL-095488, and grants from Fondation Leducq and the Totman Medical Research Trust (to M.T.N.). C.E.W. was supported by NIH Grant T32 HD041697, and W.S.C. was supported by NINDS Grant P30 NS048154. The generation of *Pkd2l1*-Cre mice was supported by Grants P30 NS048154 and P30 DC004657.

1. Huang AL, et al. (2006) The cells and logic for mammalian sour taste detection. *Nature* 442(7105):934–938.
2. Chaudhari N, Roper SD (2010) The cell biology of taste. *J Cell Biol* 190(3):285–296.
3. Liman ER, Zhang YV, Montell C (2014) Peripheral coding of taste. *Neuron* 81(5): 984–1000.
4. Thomas CJ, Lawless HT (1995) Astringent subqualities in acids. *Chem Senses* 20(6): 593–600.
5. Lyall V, et al. (2001) Decrease in rat taste receptor cell intracellular pH is the proximate stimulus in sour taste transduction. *Am J Physiol Cell Physiol* 281(3):C1005–C1013.
6. Dickman JD, Smith DV (1988) Response properties of fibers in the hamster superior laryngeal nerve. *Brain Res* 450(1-2):25–38.
7. Barretto RP, et al. (2015) The neural representation of taste quality at the periphery. *Nature* 517(7534):373–376.
8. Lin W, Ogura T, Kinnamon SC (2002) Acid-activated cation currents in rat vallate taste receptor cells. *J Neurophysiol* 88(1):133–141.
9. Ishimaru Y, et al. (2006) Transient receptor potential family members PKD1L3 and PKD2L1 form a candidate sour taste receptor. *Proc Natl Acad Sci USA* 103(33): 12569–12574.
10. Stevens DR, et al. (2001) Hyperpolarization-activated channels HCN1 and HCN4 mediate responses to sour stimuli. *Nature* 413(6856):631–635.
11. LopezJimenez ND, et al. (2006) Two members of the TRPP family of ion channels, Pkd1l3 and Pkd2l1, are co-expressed in a subset of taste receptor cells. *J Neurochem* 98(1):68–77.
12. Ugawa S, et al. (1998) Receptor that leaves a sour taste in the mouth. *Nature* 395(6702):555–556.
13. Richter TA, Dvoryanchikov GA, Roper SD, Chaudhari N (2004) Acid-sensing ion channel-2 is not necessary for sour taste in mice. *J Neurosci* 24(16):4088–4091.
14. Nelson TM, et al. (2010) Taste function in mice with a targeted mutation of the *pkd1l3* gene. *Chem Senses* 35(7):565–577.
15. Horio N, et al. (2011) Sour taste responses in mice lacking PKD channels. *PLoS One* 6(5):e20007.
16. Chang RB, Waters H, Liman ER (2010) A proton current drives action potentials in genetically identified sour taste cells. *Proc Natl Acad Sci USA* 107(51):22320–22325.
17. Kataoka S, et al. (2008) The candidate sour taste receptor, PKD2L1, is expressed by type III taste cells in the mouse. *Chem Senses* 33(3):243–254.
18. Harvey RB (1920) The relation between the total acidity, the concentration of the hydrogen ion, and the taste of acid solutions. *J Am Chem Soc* 42(4):712–714.
19. Ogiso K, Shimizu Y, Watanabe K, Tonosaki K (2000) Possible involvement of undissociated acid molecules in the acid response of the chorda tympani nerve of the rat. *J Neurophysiol* 83(5):2776–2779.
20. Richter TA, Caicedo A, Roper SD (2003) Sour taste stimuli evoke Ca^{2+} and pH responses in mouse taste cells. *J Physiol* 547(Pt 2):475–483.
21. Bushman JD, Ye W, Liman ER (2015) A proton current associated with sour taste: Distribution and functional properties. *FASEB J* 29(7):3014–3026.
22. Richter TA, Dvoryanchikov GA, Chaudhari N, Roper SD (2004) Acid-sensitive two-pore domain potassium (K2P) channels in mouse taste buds. *J Neurophysiol* 92(3): 1928–1936.
23. Lin W, Burks CA, Hansen DR, Kinnamon SC, Gilbertson TA (2004) Taste receptor cells express pH-sensitive leak K^+ channels. *J Neurophysiol* 92(5):2909–2919.
24. Zhang Z, Zhao Z, Margolskee R, Liman E (2007) The transduction channel TRPM5 is gated by intracellular calcium in taste cells. *J Neurosci* 27(21):5777–5786.
25. Clapp TR, Medler KF, Damak S, Margolskee RF, Kinnamon SC (2006) Mouse taste cells with G protein-coupled taste receptors lack voltage-gated calcium channels and SNAP-25. *BMC Biol* 4:7.
26. Huang YA, Maruyama Y, Stimac R, Roper SD (2008) Presynaptic (Type III) cells in mouse taste buds sense sour (acid) taste. *J Physiol* 586(Pt 12):2903–2912.
27. Wang YY, Chang RB, Allgood SD, Silver WL, Liman ER (2011) A TRPA1-dependent mechanism for the pungent sensation of weak acids. *J Gen Physiol* 137(6):493–505.
28. Roper SD (2007) Signal transduction and information processing in mammalian taste buds. *Pflugers Arch* 454(5):759–776.
29. Ishii S, et al. (2009) Acetic acid activates PKD1L3-PKD2L1 channel—a candidate sour taste receptor. *Biochem Biophys Res Commun* 385(3):346–350.
30. Dvoryanchikov G, Sinclair MS, Perea-Martinez I, Wang T, Chaudhari N (2009) Inward rectifier channel, ROMK, is localized to the apical tips of glial-like cells in mouse taste buds. *J Comp Neurol* 517(1):1–14.
31. Yee KK, Sukumaran SK, Kotha R, Gilbertson TA, Margolskee RF (2011) Glucose transporters and ATP-gated K^+ (KATP) metabolic sensors are present in type 1 taste receptor 3 (T1r3)-expressing taste cells. *Proc Natl Acad Sci USA* 108(13):5431–5436.
32. Hibino H, et al. (2010) Inwardly rectifying potassium channels: Their structure, function, and physiological roles. *Physiol Rev* 90(1):291–366.
33. Enyedi P, Czirják G (2010) Molecular background of leak K^+ currents: Two-pore domain potassium channels. *Physiol Rev* 90(2):559–605.
34. Wang HR, et al. (2011) Selective inhibition of the K(ir)2 family of inward rectifier potassium channels by a small molecule probe: The discovery, SAR, and pharmacological characterization of ML133. *ACS Chem Biol* 6(8):845–856.
35. Qu Z, et al. (1999) Identification of a critical motif responsible for gating of Kir2.3 channel by intracellular protons. *J Biol Chem* 274(20):13783–13789.
36. Masia R, Krause DS, Yellen G (2015) The inward rectifier potassium channel Kir2.1 is expressed in mouse neutrophils from bone marrow and liver. *Am J Physiol Cell Physiol* 308(3):C264–C276.
37. Zaritsky JJ, Eckman DM, Wellman GC, Nelson MT, Schwarz TL (2000) Targeted disruption of Kir2.1 and Kir2.2 genes reveals the essential role of the inwardly rectifying K^+ current in K^+-mediated vasodilation. *Circ Res* 87(2):160–166.
38. Zurborg S, et al. (2011) Generation and characterization of an Advillin-Cre driver mouse line. *Mol Pain* 7:66.
39. Lyall V, et al. (2006) Intracellular pH modulates taste receptor cell volume and the phasic part of the chorda tympani response to acids. *J Gen Physiol* 127(1):15–34.
40. Kumar NN, et al. (2015) PHYSIOLOGY. Regulation of breathing by CO_2 requires the proton-activated receptor GPR4 in retrotrapezoid nucleus neurons. *Science* 348(6240): 1255–1260.
41. Kinnamon SC, Roper SD (1988) Membrane properties of isolated mudpuppy taste cells. *J Gen Physiol* 91(3):351–371.
42. Kinnamon SC, Dionne VE, Beam KG (1988) Apical localization of K^+ channels in taste cells provides the basis for sour taste transduction. *Proc Natl Acad Sci USA* 85(18): 7023–7027.
43. Medler KF, Margolskee RF, Kinnamon SC (2003) Electrophysiological characterization of voltage-gated currents in defined taste cell types of mice. *J Neurosci* 23(7): 2608–2617.
44. Romanov RA, Kolesnikov SS (2006) Electrophysiologically identified subpopulations of taste bud cells. *Neurosci Lett* 395(3):249–254.
45. Perea-Martinez I, Nagai T, Chaudhari N (2013) Functional cell types in taste buds have distinct longevities. *PLoS One* 8(1):e53399.
46. Huang J, et al. (2010) Activation of TRP channels by protons and phosphoinositide depletion in *Drosophila* photoreceptors. *Curr Biol* 20(3):189–197.
47. Kubo Y, Baldwin TJ, Jan YN, Jan LY (1993) Primary structure and functional expression of a mouse inward rectifier potassium channel. *Nature* 362(6416):127–133.
48. Filosa JA, et al. (2006) Local potassium signaling couples neuronal activity to vasodilation in the brain. *Nat Neurosci* 9(11):1397–1403.
49. Dando R, et al. (2015) A permeability barrier surrounds taste buds in lingual epithelia. *Am J Physiol Cell Physiol* 308(1):C21–C32.
50. Hardie RC, et al. (2002) Molecular basis of amplification in *Drosophila* phototransduction: Roles for G protein, phospholipase C, and diacylglycerol kinase. *Neuron* 36(4):689–701.
51. Burns ME, Baylor DA (2001) Activation, deactivation, and adaptation in vertebrate photoreceptor cells. *Annu Rev Neurosci* 24:779–805.
52. Lowe G, Gold GH (1993) Nonlinear amplification by calcium-dependent chloride channels in olfactory receptor cells. *Nature* 366(6452):283–286.
53. Kurahashi T, Yau KW (1993) Co-existence of cationic and chloride components in odorant-induced current of vertebrate olfactory receptor cells. *Nature* 363(6424): 71–74.
54. Madisen L, et al. (2010) A robust and high-throughput Cre reporting and characterization system for the whole mouse brain. *Nat Neurosci* 13(1):133–140.
55. Feliciangeli S, et al. (2010) Potassium channel silencing by constitutive endocytosis and intracellular sequestration. *J Biol Chem* 285(7):4798–4805.
56. Otsu N (1979) Threshold selection method from gray-level histograms. *IEEE T Syst Man Cyb* 9(1):62–66.
57. Ma L, Xie YP, Zhou M, Chen H (2012) Silent TWIK-1 potassium channels conduct monovalent cation currents. *Biophys J* 102(8):L34–L36.
58. Zhou M, et al. (2009) TWIK-1 and TREK-1 are potassium channels contributing significantly to astrocyte passive conductance in rat hippocampal slices. *J Neurosci* 29(26):8551–8564.

Supporting Information

Ye et al. 10.1073/pnas.1514282112

SI Methods

Animals. Mouse handling, genotyping, and methods of killing were approved by the University of Southern California Institutional Animal Care and Use Committee. Mouse strains *Pkd2l1*-YFP, *Pkd1l3*$^{-/-}$ and *Trpm5*-GFP were previously described (14, 16, 25). Mouse strains *Kcnj2*$^{fl/fl}$, *Pkd2l1*-Cre are described below. *Avil*-Cre mice were a kind gift from the Peter Heppenstall Laboratory, European Molecular Biology Laboratory, Monterotondo, Rome (38). For the validation of the cell-specific expression of Cre recombinase, the two strains were each bred into a *Rosa26*^{Tdt} strain (The Jackson Laboratory; stock 007908) (54), and immunocytochemistry (see below) was used to identify the Td-Tomato–expressing cell population. To monitor expression of Cre from the *Pkd2l1* promoter in nonsour taste cells, the *Pkd2l1*-Cre::*Rosa26*^{Tdt} strain was bred into a *Trpm5*-GFP strain (25). To monitor expression of Cre from the *Avil* promoter in sour taste cells, the *Avil*-Cre::*Rosa26*^{Tdt} was bred into a *pkd211*-YFP strain (16).

***Pkd2l1*-Cre Mouse Strain.** Gene targeting was used to insert an IRES-Cre transgene immediately after the stop codon of *Pkd2l1* gene in the mouse genome. The targeting vector was constructed by cloning a 5.2-kb genomic fragment encompassing the last exon of *Pkd2l1* gene into pBluescript and inserting IRES-Cre immediately after the stop codon. A floxed-neomycin resistance cassette was cloned at a site immediately downstream of the IRES-Cre. The targeting vector was linearized by XmaI digestion and electroporated into mouse ES cells (EC7.1 line). Recombinant ES cells were selected by G418 resistance in culture, and 282 clones were isolated for PCR screening to identify correct targeting events. Two correctly targeted clones were isolated and were used for microinjection to generate germ-line chimeras, and through standard breeding, the F_1 generation of mice. To monitor expression in nonsour taste cells, the *Pkd2l1*-Cre::*Rosa26*^{Tdt} strain was bred into a *Trpm5*-GFP strain (25), and confocal images were taken, as shown in Fig. S3*C*.

Floxed *Kcnj2* Mouse Strain. Floxed *Kcnj2* mice were generated by the M.T.N. Laboratory (University of Vermont, Burlington, VT) and will be described elsewhere in more detail. In brief, the second exon of *Kcnj2* was flanked by *Lox*P sites and a downstream Neo cassette was flanked by FRT sites. The neo cassette was removed by breeding to a FLP-deleter mouse (The Jackson Laboratory). To generate a *Kcnj2* sour taste cell-specific knockout in a background of *Pkd2l1*-YFP, the *Pkd2l1*-Cre and *Pkd2l1*-YFP strains were each bred with the *Kcnj2*^{fl} strain and the offspring were further bred to generate *Pkd2l1*-YFP, *Pkd2l1*-Cre, *Kcnj2*$^{fl/fl}$ progeny. To generate a knockout of *Kcnj2* in TRPM5 cells in a background of *Trpm5*-GFP, the *Avil*-Cre strain and *Trpm5*-GFP strain were each bred with the *Kcnj2*^{fl} strain, and the offspring were further bred to generate *Trpm5*-GFP, *Avil*-Cre, *Kcnj2*$^{fl/fl}$ progeny. Genotyping methods for Pkd2l1-YFP strain were previously described (16). The primers for detecting *Cre*, *Tdt*, and *Kcnj2*^{fl} are as follows: *Cre* (GCACTGATTTCGACCAGGTT, GAGTCATCCTTAGCGCCGTA; 420-bp product), *Rosa26*^{Tdt} (CTGTTCCTGTACGGCATGG, GGCATTAAAGCAGCGTATCC; 196-bp product), *Kcnj2* distal *lox*P (TCCGATGACACTGAGAACCTGGA, TGGATGCTTCCGAGAACCTTGG; WT allele: 520 bp; floxed allele: 600 bp), *Kcnj2* neo deletion (CTGACTGAACACACAGGTCCAGGG, GGGACCATCAAGCCCTGGTAATGG; floxed allele: 800 bp; WT allele: 600 bp).

Subcloning and Heterologous Expression. $K_{IR}2.1$ was kindly provided by Zhe Lu, University of Pennsylvania, Philadelphia; $K_{IR}2.2$, $K_{IR}4.2$ were amplified from mouse skeleton muscle and kidney cDNA. The amplified fragments were inserted into pcDNA3 vector with the In-Fusion method (Clontech). KCNK1 was mutated to increase membrane trafficking (KCNK1-I293A,I294A; KCNK1-AA) (55) and was fused to GFP by removing the stop codon and inserting the gene upstream in frame with the GFP coding sequence. Clones used for recording were fully sequenced (Genewiz).

HEK 293 cells were cultured with DMEM containing 10% (vol/vol) FBS and 0.05% gentamicin. $K_{IR}2.1$, $K_{IR}2.2$, and $K_{IR}4.2$ were cotransfected with GFP (ratio 20:1), whereas KCNK1-GFP and KCNK1-AA-GFP were transfected alone, using TransIT-293 Transfection Reagent (Mirus Bio). Cells were lifted with trypsin-EDTA 24 h after transfection and used for recording within 6 h. All cell culture reagents were from Life Technologies.

Calculation of the Blocker Concentration Needed to Produce an Equivalent Magnitude Current in TRPM5 Cells as in PKD2L1 Cells. We assumed a single-site binding model for block of the K^+ channel by intracellular protons:

$$I_{\text{blocked}}/I_{\text{initial}} = 1 - \left[1/\left(1 + [H^+]_i/IC_{50}\right)\right].$$

Solving this equation for the case of the PKD2L1 cell where $I_{\text{blocked}}/I_{\text{initial}} = 0.60$ yields a value of $[H^+]_i = 1.5{*}IC_{50}$ and solving for the case of the TRPM5 cell where $I_{\text{blocked}}/I_{\text{initial}} = 0.87$ yields a value of $[H^+]_i = 6.7{*}IC_{50}$. The ratio of the two is 4.5.

Estimation of the Contribution of KCNK1 to the Taste Cell K^+ Current. We rearranged a set of linear functions assuming that the Rb^+ and K^+ inward currents are generated solely from the contributions of KCNK1 and $K_{IR}2.1$, and that the ratio of Rb^+ to K^+ permeability was preserved. Rearranging to solve for IK_{KCNK1}, the potassium current contributed by KCNK1, results in the following equation:

$$IK_{KCNK1} = IK_{\text{taste}}\ (r_{\text{taste}} - r_{KIR2.1})/(r_{KCNK1} - r_{KIR2.1}),$$

where IK_{taste} is the resting K^+ current amplitude in PKD2L1 taste cells, and r is the ratio of Rb^+ to K^+ current for KCNK1, $K_{IR}2.1$, or PKD2L1 taste cell as indicated in subscript.

RNAseq. A small region of the tongue containing circumvallate papillae and control regions devoid of taste buds was microdissected, and RNA was extracted with TRIzol (Life Technologies). Library construction and sequencing were carried out at the Norris Cancer Center Next Gen sequencing core. RNA was visualized on a Bio-Rad Experion to ensure RNA Quality Index values were greater than 8. For library construction, the Illumina TruSeq, version 2, mRNA kit was used. The protocol was followed according to manufacturer's instructions except the final number of PCR cycles was 12 and not 15. Following construction, libraries were visualized by Bioanalyzer (Agilent) using the High Sensitivity Chip and quantified for pooling and sequencing using Kapa Biosystems qPCR quantitation kit according to manufacturer's instructions. For sequencing, libraries were diluted to 16 pM, and then applied to a V3 flowcell using the Illumina cBot according to manufacturer's instructions. Sequencing was carried out on the HiSeq 2000 using HSCS, version 1.5.15.1. Image analysis and base calling were carried out using RTA 1.13.48.0, and deconvolution and fastq file

production were performed with CASAVA 1.8.2. Reads were mapped to the mouse genome (mm9) summed and converted to reads per kilobase per million reads (RPKM) using the equation: RPKM = [# of mapped reads]/([length of transcript]/1,000)/([total reads]/10^6).

Immunohistochemistry and Cell Counting. For measuring the expression of the PKD2L1-Cre reporter, circumvallate taste tissue was incubated in 4% paraformaldehyde for 1.5 h before being cryoprotected in 20% sucrose solution at 4 °C overnight. Tissue was embedded in OCT at −60 °C and sectioned at 12 μm. Slides were blocked with 2% normal donkey serum in buffer containing 0.3% Triton for 1 h before being incubated in primary antibody overnight at 4 °C and secondary antibody for 3 h at room temperature (RT). Slides were mounted with Fluoromount-G (SouthernBiotech) and imaged on a Leica confocal microscope. Hiroaki Matsunami, Duke University, Durham, NC generously provided the primary anti-PKD2L1 1:500, which was previously described (9). All *z*-stack images were acquired on a Leica confocal. To quantify immunohistochemical images, we defined a cell as a distinct shape featuring: (*i*) a clear nuclear region and (*ii*) an elongation along the pore-to-base axis of the taste bud. We thresholded images using a modified Otsu method (56) and counted positive cells by eye, tracing each through the image stack via optical dissection.

For measuring expression of the *Avil*-Cre reporter, circumvallate papillae from triple transgenic *Avil*-Cre::*Rosa26*^{Tdt}::*Pkd2l1*-YFP mice were dissected and incubated in 4% paraformaldehyde for 30 min at RT. The tissue was cryoprotected in 30% sucrose at 4 °C overnight, embedded in OCT at −80 °C and sectioned at 14 μm. Immunohistochemistry was performed by permeabilizing the tissue with 0.1% Triton X-100 for 15 min, blocking with BlockAid (Life Technologies) plus 0.1% Triton X-100 for 1 h and incubating in primary antibody overnight at 4 °C or RT for 1 h and secondary antibody at RT for 1 h. Slides were mounted with Fluoroshield (Sigma-Aldrich). The primary antibodies were chicken anti-GFP (1:1,000) (Aves Labs), guinea pig anti-TRPM5 (1:500) (24); the secondary antibodies were goat anti-chicken Alexa Fluor 488 and goat anti-guinea pig Alexa Fluor 546 (Life Technologies). All *z*-stack images were acquired on an Olympus confocal. To quantify immunohistochemical images, two observers independently scored cells as Tdt+, TRPM5+, or PKD2L1-GFP+.

Solutions for Recording KCNK1 Currents (Fig. S7). The pipette solution contained the following (in mM): 120 KAsp, 7 KCl, 8 NaCl, 10 Hepes, 2 MgATP, 0.3 GTP-Tris, 5 EGTA, 2.4 $CaCl_2$ (~100 nM free Ca^{2+}), pH 7.4 with KOH. The standard bath solution contained the following (in mM):130 NaCl, 20 TEA-Cl, 10 Hepes, 2 $CaCl_2$, 1 $MgCl_2$, pH 7.4. Rb solution contained the following (in mM): 130 RbCl, 20 TEA-Cl, 10 Hepes, 2 $CaCl_2$, 1 $MgCl_2$, pH 7.4. K solution contained the following (in mM): 130 KCl, 20 TEA-Cl, 10 Hepes, 2 $CaCl_2$, 1 $MgCl_2$, pH 7.4. CsCl was added at the concentrations indicated.

pH Imaging. Dissociated taste cells were loaded with the intracellular pH indicator pHrodo Red AM using PowerLoad concentrate accordingly to the manufacturer's instructions (Molecular Probes). TRPM5-GFP and PKD2L1-YFP cells were distinguished as previously described (21). During pH imaging, cells were excited every 5 s with light of 560 nm, and emission at 630 nm was detected by a Hamamatsu digital CCD camera attached to an Olympus IX71 microscope using a U-N31004 Texas Red/Cy3.5 filter cube (Chroma Technologies). After exposure to MA and PA (both pH balanced to 7.4 using NaOH), intracellular pH was calibrated with high K^+ solution containing the following (in mM): 140 KCl, 4.5 NaCl, 2 $CaCl_2$, 1 $MgCl_2$, 10 glucose, 10 Mes or 10 Hepes, and 0.02 nigericin (Molecular Probes), pH adjusted with NaOH to pH 6.0, 6.7, or 7.4. PHrodo Red fluorescence intensity at baseline, when exposed to MA, and when exposed to PA was converted to pH_i using linear calibration curves constructed for each cell using fluorescence intensity data in the presence of calibration solutions under the assumption that $pH_i = pH_o$.

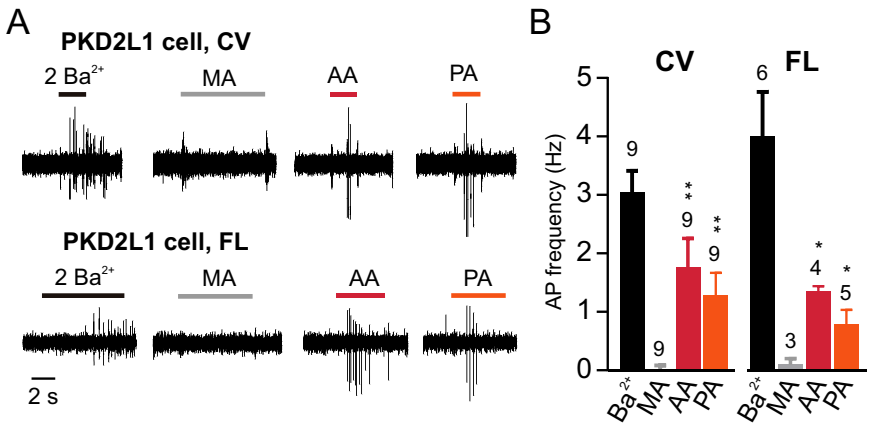

Fig. S1. Intracellular acidification evokes action potentials in dissociated PKD2L1 cells from both CV and foliate. (*A*) Action potentials were evoked in a PKD2L1 cells isolated from circumvallate and foliate papillae in response to 100 mM acetic acid (AA) and propionic acid (PA), adjusted to pH 7.4. Control stimuli were 100 mM methanesulfonic acid (MA), or 2 mM Ba^{2+}. (*B*) Average data from experiments as in *A*. By two-way ANOVA, there was a significant difference in the response to different acids (MA, AA, and PA) ($P < 0.01$) but no difference between the two taste fields ($P = 0.41$). Asterisks indicate *P* value from Student's test against MA in each cell type. $*P < 0.05$, $**P < 0.01$.

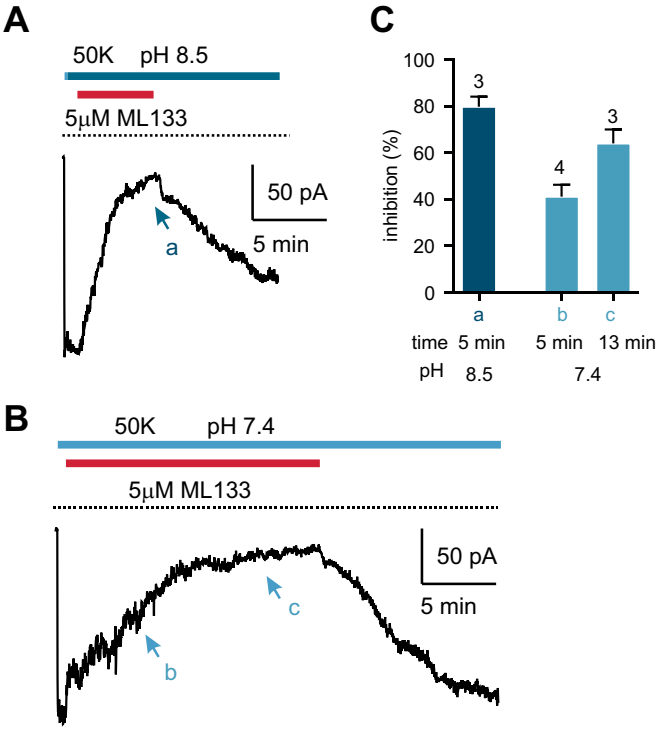

Fig. S2. Block by ML133 of the resting K^+ current in PKD2L1 taste cells is pH dependent. (*A* and *B*) The block of resting K^+ current in PKD2L1 cells by ML133 was extracellular pH dependent. At pH 8.5 (*A*), the block by 5 μM ML133 was faster than that at pH 7.4 (*B*). (*C*) Average data of cells shown in *A* and *B*. The time points the block efficiency was measured are arrowed in the trace in *A* and *B*.

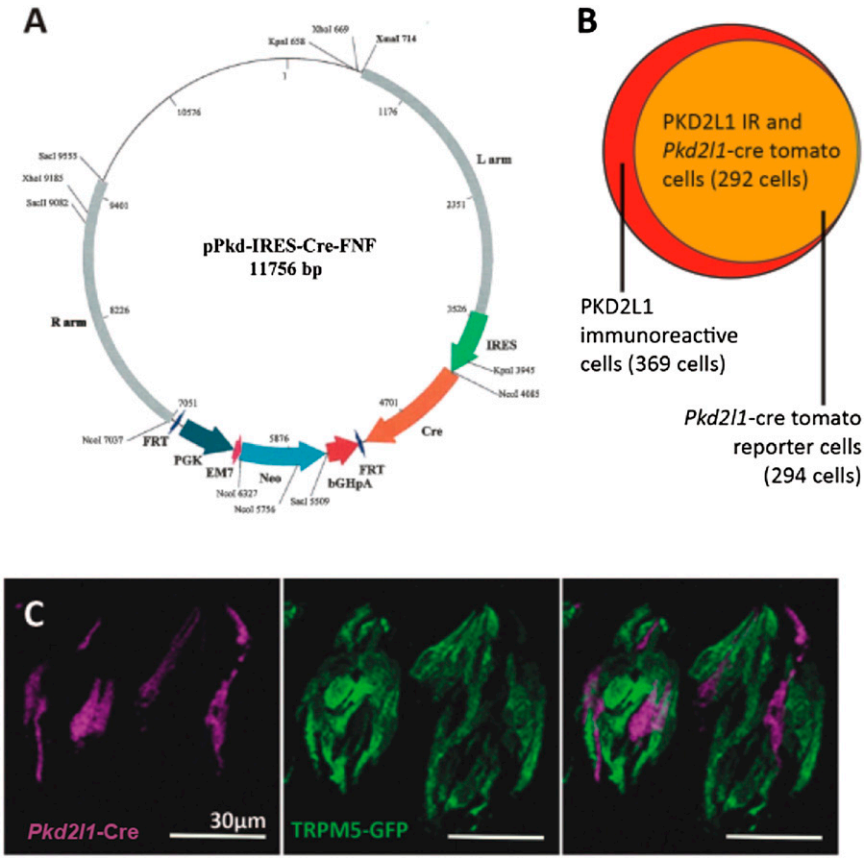

Fig. S3. *Pkd2l1*-Cre mouse strain. (*A*) Map of the *Pkd2l1*-cre plasmid used to generate the transgenic mouse strain. (*B*) A Venn diagram of count data comparing PKD2L1 immunoreactivity (red circle) to *Pkd2l1*-Cre tomato reporter positive cells (yellow circle). Overlap shown in orange. Cre reporter efficiency, as determined by the tomato reporter fluorescence, is ~79% in the circumvallate taste tissue. (*C*) Confocal image *z* stacks of circumvallate taste buds from a triple-transgenic *Pkd2l1*-Cre, *Rosa*^{Tdt}, *Trpm5*-GFP mouse. Tomato reporter expression is displayed in magenta, and *Trpm5*-driven GFP fluorescence is displayed in green. Tomato reporter fluorescence and *Trpm5*-driven GFP fluorescence do not coincide. (All scale bars: 30 μm.)

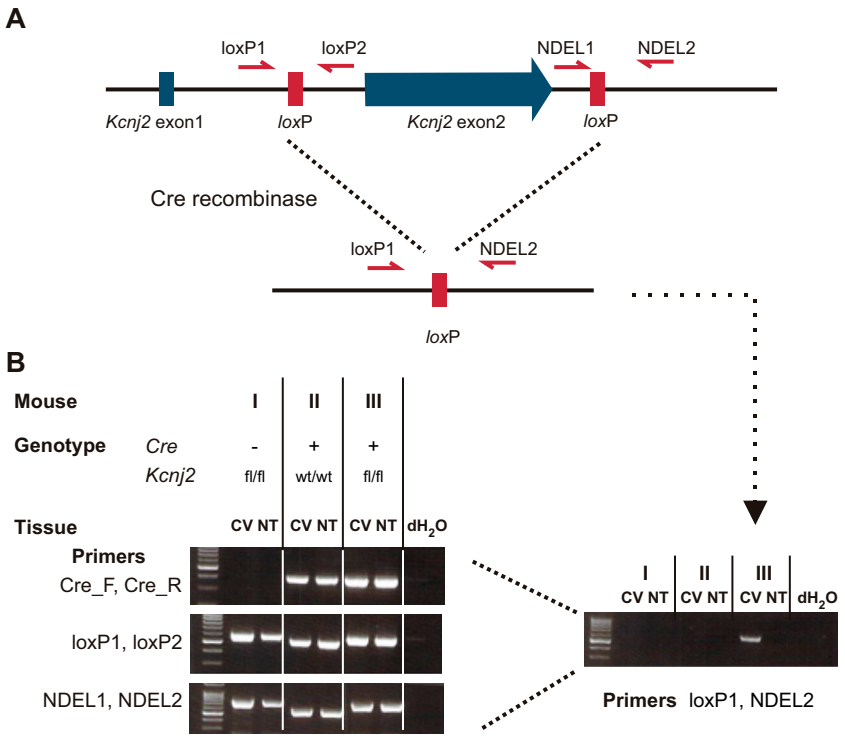

Fig. S4. Floxed *Kcnj2* is specifically excised in Cre-expressing tissue. (*A*) The design for Cre-*lox*P dependent tissue-specific knockout of *Kcnj2*, the gene that encodes $K_{IR}2.1$. Exon2 of *Kcnj2*, which covers the entire coding sequence, was floxed. Primers that were used to genotype animals are indicated. (*B*) PCR of genomic DNA from circumvallate (CV) and nontaste (NT) tissues of mice representing the three genotypes indicated. The left panel shows the results of genotyping the mice using the indicated primer pairs. Note that, for this analysis, the source of the genomic DNA is irrelevant. The right panel shows the results of a PCR designed to test for the deletion of exon 2, which is only expected to occur in taste tissue from *Pkd2l1*-Cre::*Kcnj2*$^{fl/fl}$ mice. The same template DNA was used as in the right panel, which therefore serves as a control for this experiment.

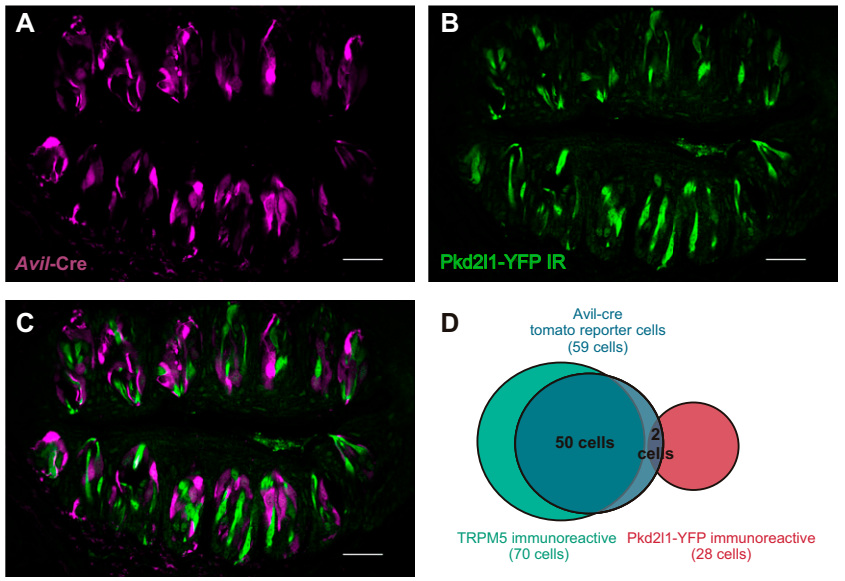

Fig. S5. Distribution of *Avil*-Cre in taste cells. (*A*–*C*) Confocal images of the same field of circumvallate taste buds from an *Avil*-Cre::*Rosa26*^{tdT}::*Pkd2l1*-YFP mouse as in Fig. 7. The reporter expression is displayed in magenta, and YFP immunoreactivity, which reflects the expression pattern of *Pkd2l1*, is displayed in green. Note that there is very little overlap between Cre reporter expression and and YFP immunoreactivity (*C*). (Scale bar: 30 μm.) (*D*) A Venn diagram of count data showing TRPM5-immunoreactive cells (green circle, as in Fig. 7*A*), *pkd2l1*-YFP–immunoreactive cells (blue circle), and *Avil*-Cre tomato reporter-positive cells (red circle). The Cre reporter was detected in ∼71% of TRPM5 cells and 8% of PKD2L1 cells.

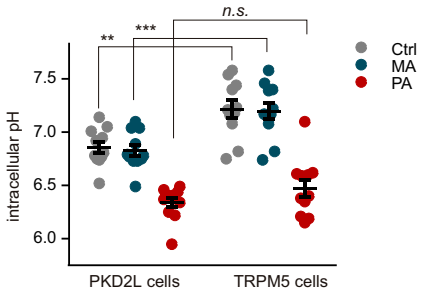

Fig. S6. The intracellular pH to which TRPM5 cells are acidified by weak acids is similar to that of PKD2L1 cells. Scatter plot of intracellular pH from imaging of cells loaded with pHrodo Red. Cells were sequentially exposed to bath solution (Tyrode's), 100 mM methanesulfonic acid (MA), and 100 mM propionic acid (PA), all pH 7.4. Intracellular pH was calibrated as described in *Methods*. By two-way ANOVA, there was a significant difference across the conditions ($P < 0.0001$) and across cell types ($P < 0.01$). Post hoc analysis with Sidak's test corrected for multiple comparisons showed no significant difference between cell types in response to the weak acid, PA ($P = 0.43$). As previously reported (21), the resting pH of the two cell types was significantly different as was the pH in the presence of MA. Note that MA was used as a control and was not expected to cause a change in pH from resting conditions. $^{**}P < 0.01$, $^{***}P < 0.001$.

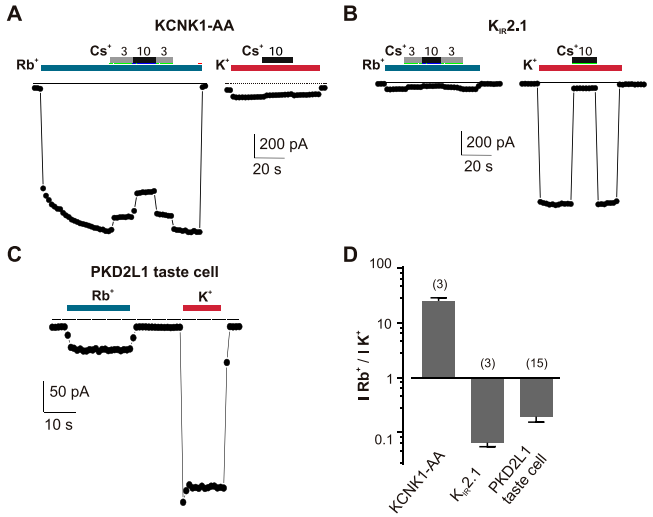

Fig. S7. KCNK1 does not contribute to the resting K^+ current in PKD2L1 cells. (*A*) The current recorded from a KCNK1-AA-GFP–transfected HEK cell under conditions designed to unmask the current. Note that in 130 mM Rb^+ (with 20 mM TEA), the current magnitude was much larger than that in 130 mM K^+ extracellular solution (also with 20 mM TEA) as previously reported (57). Cs^+ was not an effective blocker of KCNK1 current (58). (*B*) Same experiments as in *A* performed with a $K_{IR}2.1$-transfected cell. Note that the current in Rb^+ is much smaller than that in K^+ solutions, and that Cs^+ blocks the current effectively. (*C*) The current recorded in a PKD2L1 taste cell. Note that the current magnitude in Rb^+ is smaller than that in K^+, similar to the $K_{IR}2.1$-mediated current. (*D*) The ratios of current in 130 mM Rb^+ (I_{Rb}^+) to that in 130 mM K^+ (I_K^+) for KCNK1-AA, $K_{IR}2.1$, and PKD2L1 taste cells. Using these data, we estimated the contribution of KCNK1 to the taste cell K^+ current by rearranging a set of linear functions assuming that the inward currents in high Rb^+ and K^+ are generated solely from the contributions of KCNK1 and $K_{IR}2.1$ (*SI Methods*). This calculation showed that KCNK1 accounts for no more than 1% of the resting K^+ current.